DEVELOPMENT OF A THEORY OF THE SPECTRAL REFLECTANCE OF MINERALS

by

J. R. ARONSON AND A. G. EMSLIE

OCTOBER 1969

NAS 9-8396

ADL 70544

Arthur D. Little, Inc.

NASA CR 102009

DEVELOPMENT OF A THEORY OF THE SPECTRAL REFLECTANCE OF MINERALS

By

J. R. Aronson and A. G. Emslie

Arthur D. Little, Inc.
Cambridge, Massachusetts 02140

Prepared for

National Aeronautics and Space Administration
Manned Spacecraft Center
Houston, Texas 77058

FINAL REPORT

Contract No. NAS 9-8396
ADL C-70544

October 1969

Arthur D Little, Inc.

ACKNOWLEDGMENT

We are indebted to Dr. R. K. McConnell and B. M. Sather for their invaluable contributions to the computer programming; to P. F. Strong for his many helpful suggestions in the development of the theory; and to P. C. von Thüna for his expert assistance in the design, development, and testing of the experimental apparatus. In addition, we are grateful to Dr. T. P. Rooney of Air Force Cambridge Research Laboratories for providing some unpublished experimental data on the spectral reflectance of quartz and corundum powders and for making computer facilities available.

TABLE OF CONTENTS

TABLE OF CONTENTS (continued)

LIST OF FIGURES

LIST OF FIGURES (continued)

I. INTRODUCTION

The task to which we have addressed ourselves in this research program is incredibly complex. What we are attempting to construct is a quantitative theory of the reflectance (or emittance) spectra of mixtures of solids. In particular, we are interested in the spectral properties of minerals as they appear viewed by remote techniques. A completely rigorous solution of the problem is out of the question at the present time. However, if it is recognized that in many of the details involved it is possible to make some simplifying approximations, many of which result from statistical considerations, considerable progress can be made.

The work reported here has been effectively a continuation and extension of our previous research in the area of the reflectance spectra of rocks and minerals. Many of the results of our earlier studies have been published before[1-5] but some of that material will be included in this report for the sake of a coherent presentation. The basic problem is that of remote determination of the composition of planetary surfaces. It has long been known that infrared spectra provide diagnostic compositional information for homogeneous solids. However, the reflectance or emittance spectra of a given material under various physical conditions such as changed particle size of particulate samples and altered surface roughness can be quite different. In different spectral regions a given reflectance peak may increase or decrease in intensity as the particle size of the material is decreased.[6,7] Further, a continuing reduction of the particle size may reverse the trend even for a single spectral feature.[8] When mixtures of materials are involved, it is clear that a linear superposition of the spectra of the components is not generally applicable. Nonetheless identification of rocks and minerals even in particulate form have been successfully accomplished by remote spectroscopy.[9,10] A considerable body of experimental evidence concerning these complications exists[3,5-8] but to date no satisfactory quantitative theoretical treatment has been available.

It is clear from these data that an adequate theoretical treatment must be able to explain both increases and decreases in reflectance that occur as a function of a monotonically varying particle size, for example.

Our theoretical treatment has been premised on a belief that all of the spectral details for mixtures under varying physical conditions can be explained using a relatively small number of parameters. These parameters are the radiation wavelength, the wavelength dependent refractive index and absorption coefficient, the volume fractions of the components, a measure of the particle size such as diameter (which may require refinement to three dimensions, depending on particle shape) and a factor relating to surface roughness.

Our technique has been to examine experimental data, both from the literature and that we have generated ourselves, and to then test any theoretical treatment against these data. This procedure may suggest critical experiments to be carried out. The process can then be iterated. The definition of such critical experiments is quite difficult for a number of reasons. The most important is the requirement that the samples be well characterized with regard to the parameters listed above. Unfortunately, there are relatively few materials for which the optical constants are well known over a broad spectral region. When the requirement of known and narrow particle-size distribution (so as to be able to predict changes with particle size) is added, one has very few materials with which to work. For these reasons we have chosen to work extensively with corundum and quartz.

II. THE THEORY OF REFLECTANCE

A. GENERAL APPROACH

In remote infrared spectrometry of a planetary or terrestrial surface, one would generally measure the radiation coming from a patch of terrain vertically below the instrument. Therefore the quantity of interest is the normal emittance of the surface. By Kirchhoff's law the normal emittance is equal to $1-A$, the normal reflectance, i.e., the total reflection coefficient for a collimated infrared beam incident normally on the surface. From the theoretical point of view it is easier to calculate the normal reflectance than the normal emittance.

Reflection of a beam incident normally on a powdered sample involves a number of interacting effects. A fraction R_e of the beam is reflected by the externally exposed facets of the powder particles. The remaining fraction $1-R_e$ of the beam enters the sample and is rapidly converted from collimated radiation to diffuse radiation by multiple reflection and refraction by the particles. At greater depths in the powder the radiation is in a state of statistical equilibrium in which the ratio of outward to inward directed flux is independent of depth. This ratio is the volume reflectance R_v.

Some of the backscattered diffuse radiation returns to the surface of the powder where it is partially reflected owing to the discontinuity in optical properties between the powder and the external space. We call this internal reflectance R_i.

The overall reflectance R of the powder is related to the three reflectances R_e, R_v, and R_i by the formula*

$$R = R_e + \frac{(1 - R_e)(1 - R_i)R_v}{(1 - R_i R_v)}\left(\frac{2}{3 - R_v}\right) \qquad (1)$$

*Derivations of this and other formulas are given in the Appendix.

where the factor $2/(3-R_v)$ allows for the conversion of the radiation from collimated to diffuse. For the case of diffuse incident radiation this factor is absent.

The external and internal surface reflectances R_e and R_i depend on the geometrical structure of the powder, the degree of roughness of the surface, the particle sizes and shapes, the optical constants of the particles, and the wavelength of the radiation. The magnitudes of R_e and R_i depend strongly on whether the particles of the powder reflect coherently or incoherently, i.e., on whether the structure of the powder is on a scale that is small or large compared with the wavelength. We therefore need two quite different methods of calculation for the two cases--a fine-particle theory and a coarse-particle theory. In both theories R_i is usually much larger than R_e, which can often markedly reduce the contribution of R_v to the total reflectance owing to the $1-R_i$ factor in Equation (1). For this reason we feel that inclusion of the effect of internal surface reflection is very important, although it is often neglected in the literature.

To calculate R_e and R_i we have to know the geometry of the surface. For simplicity, we assume that the surface is what one would obtain by slicing through the powder without displacing any particles. In the coarse-particle theory R_e is then the average Fresnel reflection coefficient at normal incidence for all the exposed facets. R_i is the average Fresnel coefficient for diffuse radiation incident internally on the same facets. On the other hand, in the fine-particle theory we first find the volume average of the optical constants by means of the Lorentz-Lorenz theory[1] and then calculate the two Fresnel reflection coefficients as though the surface were flat and continuous.

The main task is the calculation of the volume reflectance R_v. It is very convenient to express this quantity first in terms of the macroscopic scattering and absorption coefficients S and K of the Schuster[11] or Kubelka-Munk[12] theory. The Kubelka-Munk theory gives

the formula[2]

$$R_v = 1 + \frac{K}{S} - \sqrt{\frac{K^2}{S^2} + 2\frac{K}{S}} \qquad (2)$$

which shows that R_v depends only on the ratio of the absorption and scattering coefficients and not on their absolute values.

The difficult part of the problem is the calculation of S and K from the geometry and optical constants of the powder, and the wavelength of the radiation. One approach, which has been tried by several authors, is to use what we will call the "particle model." In this model one starts with the known angular scattering distribution (phase function) for a single particle irradiated by a plane wave. One then calculates the effect of successive scattering by the particles in a sample either by a Monte Carlo method or by the theory of Chandrasekhar.[13] These methods are certainly valid for widely spaced particles, as in a cloud of water droplets. However, in the case of nonspherical particles in contact with each other, as in a powder, the particle model is of doubtful validity for several reasons. First, there is difficulty with the very concept of a plane wave incident on a given particle when the particle is closely surrounded by other particles. Second, the wave is not scattered independently by the particles but rather by groups of closely packed particles acting cooperatively. Third, the single particle phase function is known accurately only for spherical particles (Mie theory).[14] For large particles the Mie theory requires the computation of a very large number of terms of a series of oscillatory functions. The result of the computation is a phase function containing a great amount of fine structure that pertains only to spherical particles. Particles of even slightly different shape have quite different fine structures. Therefore, most of the computer time is spent wastefully. For closely spaced fine particles the Mie theory phase function is simple but the assumption of noncooperative scattering is invalid. Therefore a single particle phase function is a poor approximation.

To avoid these difficulties of the Mie theory method we take an entirely different approach, in the case of coarse particles, which can be called the "random interface" model. Instead of considering a space full of particles, we consider a space full of interfaces. Any interface separates a region of refractive index $n_j - ik_j$ from a region of index 1, where j specifies one of the minerals of which the powder is composed. The assumption of randomness of the interfaces is a simplification required to make the calculations tractable. The assumption of interfaces only with vacuum would only be valid for relatively porous media where particles are presumably only in point contact. The idea is that if a line is drawn through the powder in any direction the points of intersection of the line with interfaces are randomly distributed on the line. The average number of intersections per unit length of line depends on the sizes and volume fractions of the various types of particles in the powder.

As with the calculation of surface reflectance we need both coarse- and fine-particle theories. For coarse particles we use geometrical optics and calculate the average phase functions for both reflection and refraction at a randomly oriented interface. Knowing the two phase functions for each type of mineral we then determine the diffuse backscattering coefficient S by summing the contributions from all minerals and voids for both reflection and refraction. In making the summations we weight the contributions in proportion to the diffuse radiation intensity in each mineral, i.e., in proportion to n_j^2. The absorption coefficient K is calculated from the absorption indices k_j of the various minerals again with n_j^2 weighting factors and with allowance for the average slant path appropriate to diffuse radiation. In performing these calculations we consider the radiation intensity in any direction to be a volume average of the radiation intensities in the various minerals, including vacuum, with weighting factors of n_j^2 as mentioned above.

In the coarse-particle model the scattering from the various interfaces is added incoherently. This is valid when the phases of the scattered waves are random, which happens in those regions of the spectrum where the wavelength in the material is shorter than about twice the mean spacing of the randomly distributed interfaces. At points in the spectrum where the wavelength is longer than this, one must use the fine-particle model in which scattered amplitudes rather than intensities are added.

We have tried two approaches for calculating the fine-particle scattering. In the first approach we consider the random interfaces to be equivalent to a superposition of a large number of sinusoidally varying contributions to the refractive index relative to a mean index given by the Lorentz-Lorenz theory. Each sinusoidal component acts like a set of crystal planes and produces a Bragg reflection of the incident radiation. The sum (actually an integral) of the intensities of all the Bragg reflections gives the phase function for the fine-particle scattering. The phase function can be expressed in terms of the autocorrelation function of the refractive index distribution in the powder.

The second approach to the fine-particle theory is an extension of the Lorentz-Lorenz theory of the dielectric constant. It is a co-operative particle model that allows for the presence of neighboring particles in the calculation of the scattering by a given particle. The method permits calculation of the scattering by closely spaced ellipsoidal particles with random orientation as well as by spherical particles.

B. SURFACE REFLECTANCES R_e AND R_i

1. Coarse-Particle Model

In the coarse-particle model we assume for ease of calculation that the surface of the powder is what would be obtained if the powder

were sliced by a plane. Thus the assumed surface is a plane consisting of facets. We assume further that radiation reflected from other parts of the surface layer of particles, either externally or internally, is to be included in the volume part of the scattering. Under these conditions the external surface reflectance is taken to be the normal incidence Fresnel reflectance averaged over all the facets, i.e.,

$$R_e = \sum_j f_j R_{e,j} \tag{3}$$

where $R_{e,j}$ is the reflectance of mineral of type j, given by

$$R_{e,j} = \frac{(n_j - 1)^2 + k_j^2}{(n_j + 1)^2 + k_j^2} \tag{4}$$

The weighting factors f_j are the volume fractions of the various minerals in the powder. Under our assumption about the nature of the surface the f_j are also the area fractions of the different kinds of facets.

The internal surface reflectance R_i is the diffuse internal reflectance of the facets averaged with respect to both the volume fractions f_j and the radiation intensities I_j in the various kinds of particles:

$$R_i = \frac{\sum_j f_j I_j R_{i,j}}{\sum_j f_j I_j} \tag{5}$$

where $R_{i,j}$ is the diffuse internal reflectance for a facet of type j.

For diffuse radiation the intensity I_j is approximately proportional to n_j^2. Therefore the formula for R_i can be written as

$$R_i = \frac{\Sigma\, f_j n_j^2 R_{i,j}}{\Sigma\, f_j n_j^2} \tag{6}$$

The quantity $R_{i,j}$ is the internal Fresnel reflectance for mineral j averaged over all angles of incidence:

$$R_{i,j} = \frac{1}{\pi} \int_{\theta=0}^{\pi/2} \frac{[R_{i,j,\parallel} + R_{i,j,\perp}]}{2} \cos^2\theta d\omega \tag{7}$$

where θ is the angle of incidence on the facet, $d\omega$ is an element of solid angle, and $R_{i,j,\parallel}$ and $R_{i,j,\perp}$ are the usual Fresnel reflectances for the parallel and perpendicular directions of the polarization of the radiation. In applying the Fresnel formulas in our case of internal reflection in an absorbing medium we assume that the reflectances depend only on the relative index of refraction between the medium and vacuum. Thus we evaluate the reflectances $R_{i,j,\parallel}$ and $R_{i,j,\perp}$ as though the radiation were incident in a vacuum on a medium of complex index $n_j'-ik_j'$, where n_j' and k_j' are the real and imginary parts of $1/(n_j-ik_j)$.

2. Fine-Particle Model

When the structure of the powder is on a scale that is small compared with the wavelength of the radiation it is no longer correct to consider the surface reflection to be caused by the independent reflection of individual surface facets. Instead, owing to the effect of phase coherence, one must attribute the reflection to the discontinuity in the "average" complex refractive index at the surface of the medium. The proper average is one that takes into account the interactions of the particles on each other. Lorentz and Lorenz have considered this problem in connection with the dielectric constant of a medium composed of spherically symmetrical molecules of given electric polarizability α_p. They derived the well-known formula

$$\frac{\varepsilon - 1}{\varepsilon + 2} = \frac{3\alpha_p}{4\pi} \eta \qquad (8)$$

for the dielectric constant ε of the medium, where η is the number of molecules per unit volume. One can easily extend the Lorentz-Lorenz formula to the case of a mixture of molecules:

$$\frac{\varepsilon - 1}{\varepsilon + 2} = \sum_j \frac{3\alpha_{p,j}}{4\pi} \eta_j \qquad (9)$$

This expression can be put in the form of a mixing rule for the dielectric constant:

$$\frac{\varepsilon - 1}{\varepsilon + 2} = \sum_j f_j \left(\frac{\varepsilon_j - 1}{\varepsilon_j + 2} \right) \qquad (10)$$

where ε_j is the dielectric constant of a medium composed of molecules of type j only, and f_j is the volume fraction of such molecules in the mixture.

We now assume that the Lorentz-Lorenz theory can be extrapolated from molecules to small particles. We then obtain, on substituting $\varepsilon = (n-ik)^2$ and $\varepsilon_j = (n_j - ik_j)^2$ for the dielectric constants in terms of the complex refractive indices:

$$\frac{(n - ik)^2 - 1}{(n - ik)^2 + 2} = \sum_j f_i \frac{(n_j - ik_j)^2 - 1}{(n_j - ik_j)^2 + 2} \qquad (11)$$

On solving this equation for n-ik one must select the root of $(n-ik)^2$ that lies in the fourth quadrant in order that both n and k are positive.

We calculate the external and internal reflectances R_e and R_i in the same way as in the coarse-particle model except that we now consider the powder as a homogeneous medium with complex index n-ik.

We have generalized the Lorentz-Lorenz theory to the case of ellipsoidal particles, which enables reflectances to be calculated for needle-shaped or disk-shaped particles. The derivation is given in the Appendix.

3. Bridging between Coarse- and Fine-Particle Models

When the wavelength approaches the particle size the formulas of the coarse-particle model overestimate the values of R_e and R_i owing to neglect of the effect of wave interference between the outermost facets of the powder particles and the next layer of facets. In order to correct for this effect approximately and thereby help to bridge from the coarse- to the fine-particle model we multiply both R_e and R_i by an interference factor F. This factor is based on the usual formula for the normal incidence reflection coefficient R of a film of thickness d, which has the form

$$R = \frac{4\,R_o \sin^2\left(\frac{2\pi nd}{\lambda_o}\right)}{(1 - R_o)^2 + 4\,R_o \sin^2\left(\frac{2\pi nd}{\lambda_o}\right)} \tag{12}$$

where R_o is the Fresnel reflectance of one surface of the film, n is the refractive index of the medium, and λ_o is the free space wavelength. For small values of $2\pi nd/\lambda_o$ this expression becomes

$$R \approx \frac{R_o}{\left(1 - R_o\right)^2\left(\frac{\lambda_o}{4\pi nd}\right)^2} \tag{13}$$

For large values of $2\pi nd/\lambda_o$ the coarse-particle theory is valid and the reflectance should have the value R_o. A simple expression that has the correct behavior is

$$R = \frac{R_o}{1 + \left(1 - R_o\right)^2 \left(\frac{\lambda_o}{4\pi nd}\right)^2} \qquad (14)$$

Therefore we assume for the interference factor the form

$$F = \frac{1}{1 + \left(1 - R_o\right)^2 \left(\frac{\lambda_o}{4\pi nd}\right)^2} \qquad (15)$$

C. VOLUME REFLECTANCE R_v

1. Coarse-Particle Model

The volume reflectance depends only on the ratio K/S of the absorption and backscattering coefficients. For coarse particles we calculate K and S by means of our random interface model. To do this we assume that the radiation in the regions between adjacent interfaces is approximately diffuse and of intensity proportional to n_j^2. We assume furthermore that K and S are independent of each other, i.e., that K can be calculated as if there were no reflection or refraction and S can be calculated as if there were no absorption.

To calculate K we consider a typical ray of intensity I_j traversing a region j at an angle θ with respect to the x-axis, which is normal to the surface of the powder. In advancing a small distance ds the ray suffers a loss in intensity of $4\pi k_j I_j dx/\lambda_o \cos\theta$ where λ_o is the free space wavelength of the radiation. To obtain the average loss we average this quantity over the forward hemisphere with a weighting factor of $\cos\theta$. The result is $8\pi k_j I_j dx/\lambda_o$ which indicates that the effective slant path for diffuse radiation is 2dx. Next we average spatially, taking $I_j \propto n_j^2$ and allowing for the various volume fractions f_j. Then, since K is the fractional loss in intensity per unit distance in the x-direction, we obtain:

$$K = \frac{8\pi}{\lambda_o} \frac{\sum_j k_j f_j n_j^2}{\sum_j f_j n_j^2} \tag{16}$$

The backscattering coefficient S is the sum of contributions from both reflection and refraction by the random interfaces. An interface between mineral j and vacuum can reflect either externally or internally. We denote the external and internal reflectances averaged over all orientations of the interface, relative to an incident ray, by $\bar{R}_{e,j}$ and $\bar{R}_{i,j}$. The average reflectance $\bar{R}_j$ for an interface of type j is the sum of $\bar{R}_{e,j}$ and $\bar{R}_{i,j}$ weighted with respect to the external and internal intensities I_o and I_j, which are in the ratio 1 to n_j^2. Therefore

$$\bar{R}_j = \frac{\bar{R}_{e,j} + n_j^2 \bar{R}_{i,j}}{1 + n_j^2} \tag{17}$$

We now assume that for a given incident ray direction the rays reflected by a random interface, either externally or internally, are approximately isotropic. Then for any incident ray one half of the reflected radiation is backscattered. The contribution to S from j-type interfaces is therefore

$$S_j = \frac{1}{2} (2N_j) \bar{R}_j = N_j \bar{R}_j \tag{18}$$

where N_j is the average number of j-type interfaces per unit length of any line drawn through the powder. The factor of 2 multiplying N_j arises, as in the calculation of K above, from averaging over the diffuse incident radiation. The total backscattering coefficient due to reflection is

$$S_{\text{reflection}} = \sum_j F_j \frac{N_j (\bar{R}_{e,j} + n_j^2 \bar{R}_{i,j})}{1 + n_j^2} \tag{19}$$

where we have included the same interference factor F_j as in the surface reflection to correct approximately for destructive interference when the wavelength approaches the particle size.

The contribution of refraction to S is found in the following way. A given ray on striking a type-j interface is refracted through some angle ϕ from its original direction. The maximum angle ϕ_m is, from Snell's law of refraction, given by the relation

$$\cos\phi_m = \frac{1}{n_j} \qquad (n_j > 1) \tag{20}$$

If $n_j < 1$, the right-hand side must be replaced by n_j. Since the orientation of the interface is random, the refracted rays fill a cone of half angle ϕ_m. Although the intensity of the radiation in the cone varies somewhat with the angle from the axis of the cone we assume, in order to obtain an analytical expression for the fraction f_b of the incident radiation that is backscattered, that the refracted intensity is uniform over the cone. Under these conditions we find (see Appendix) for f_b the formula

$$f_b = \frac{\pi - 2\cos\phi_m \cos^{-1}\left(\frac{\tan\chi}{\tan\phi_m}\right) - 2\sin^{-1}\left(\frac{\sin\chi}{\sin\phi_m}\right)}{2\pi(1 - \cos\phi_m)} \tag{21}$$

for $\chi < \phi_m$ where χ is the angle that the incident ray makes with a plane parallel to the surface of the powder. For $\chi > \phi_m$ there is no contribution to the backscattering since all rays in the refracted cone lie in the forward hemisphere.

We find the backscattering coefficient for refraction by j-type interfaces by integrating f_b over all incident rays for which $\chi > \phi_m$:

$$S_j = \int_{\chi=0}^{\phi_m} f_b(1 - \bar{R}_j)(N_j/\sin\chi)(\sin\chi \; d\omega/\pi) \qquad (22)$$

In the integrand $1-\bar{R}_j$ is the transmission factor, $N_j/\sin\chi$ is the average number of type-j interfaces encountered by a slant ray per unit distance measured in the forward direction, and $(\sin\chi \; d\omega/\pi)$ is the fraction of the incident diffuse radiation in an element of solid angle $d\omega = 2\pi \cos\chi \; d\chi$.

On substituting for f_b, carrying out the integration and summing over the different types of interface, we find for the total backscattering coefficient due to refraction:

$$S_{refraction} = \sum_j N_j(1 - \bar{R}_j) \frac{2}{\pi} \frac{\sin\phi_{m,j} - \phi_{m,j} \cos\phi_{m,j}}{1 - \cos\phi_{m,j}} \qquad (23)$$

where $\cos\phi_{m,j} = \frac{1}{n_j} \qquad (n_j > 1)$ (24)

$= n_j \qquad (n_j < 1)$

and $\bar{R}_j$ is given by Equation (17).

It is to be noted that we do not apply here an intensity weighting factor n_j^2 for internally incident rays as we did in the case of reflection. The reason is that the external and internal diffuse transmission factors are approximately in the ratio n_j^2 : 1 which just balances out the intensity ratio between the two sides of the interface.

The total backscattering coefficient S is the sum of contributions from reflection and refraction by the random interfaces:

$$S = S_{reflection} + S_{refraction} \qquad (25)$$

The number of interfaces per unit length N_j in the expressions for $S_{reflection}$ and $S_{refraction}$ is related to the size d; and the volume fraction f_j of particles of material j. The relationship is derived as follows. The average number of particles intercepted per unit length of an arbitrary straight line is $n_j\sigma_j$, where n is the number of particles per unit volume and σ_j is the average cross-sectional area. Since each particle accounts for two interfaces, we have

$$N_j = 2\, n_j \sigma_j \tag{26}$$

The particle density n_j is related to the particle volume v_j and the volume fraction f_j by the relation

$$f_j = n_j v_j \tag{27}$$

For convex particles the cross section σ_j is related in a simple way to the surface area A_j of the particle. An element dA_j of the surface contributes to σ_j an average amount

$$d\sigma_j = \int_{\theta=0}^{\pi/2} dA_j \cos\theta \frac{d\omega}{4\pi} = \frac{1}{4} dA_j \tag{28}$$

where θ is the angle between the direction of the arbitrary straight line and the normal to dA_j and $d\omega$ is an element of solid angle. On adding the average contributions from all elements of area on the surface of the particle we get

$$\sigma_j = \frac{1}{4} A_j \tag{29}$$

On eliminating σ_j and n_j from the equations for N_j, f_j, and σ_j we arrive at the required relation

$$N_j = \frac{f_j A_j}{2v_j} \tag{30}$$

For rectangular particles of dimensions a, b, c this formula gives the result

$$N_j = f_j\left(\frac{1}{a} + \frac{1}{b} + \frac{1}{c}\right) \tag{31}$$

In the present work we are concerned first with quartz particles of random shape, represented by cubes of edge c_j, and second with corundum particles, which are platelets with edge lengths a_j, b_j, d_j approximately in the ratio 5:5:1. For these particles the formula gives $N_j = 3f_j/d_j$ and $N_j = 1.4\ f_j/d_j$, respectively. To allow for the considerable range in particle shapes and sizes in any given powder sample and for the effect of agglomeration of the particles, which is greater for corundum than for quartz, we will assume for both kinds of particles that $N_j = 2\ f_j/d_j$.

2. Fine-Particle Model

When the particle size is of the order of the wavelength or smaller we must use wave optics instead of geometrical optics in the calculation of K and S. To do this we return to the Lorentz-Lorenz theory already introduced in connection with the surface reflection of a fine powder. The absorption coefficient K of the medium is calculated from the imaginary part of the Lorentz-Lorenz refractive index. The scattering coefficient S depends on the local fluctuations of index relative to the Lorentz-Lorenz index.

Equation (11) gives the complex index n-ik of the powder according to the Lorentz-Lorenz method of averaging. The absorption coefficient α for a plane wave is

$$\alpha = \frac{4\pi k}{\lambda} \tag{32}$$

where λ_o is the free-space wavelength of the radiation. To calculate K from α we depart from the continuous-angle method used in the coarse-particle model and use instead the discrete-angle, six-beam method of Conel[15] which we will require to make the fine-particle calculation of S tractable.

In the six-beam method the diffuse radiation is represented at every point in the medium by six mutually orthogonal beams all inclined at an angle of $\cos^{-1}(1/\sqrt{3})$ (about 55°) to the x-axis. The incremental slant path is therefore $\sqrt{3}\,dx$ in this model, whereas the average slant path in the continuous-angle model is 2 dx. Therefore K is now given by the formula

$$K = \sqrt{3}\,\alpha = \frac{4\pi\sqrt{3}\,k}{\lambda_o} \tag{33}$$

It is worth noting that since S will also contain the slant factor $\sqrt{3}$, R_v is not affected by the change in value of this factor since it depends only on the ratio K/S.

In the fine-particle model, scattering arises basically from fluctuations in the Lorentz-Lorenz average index m = n-ik owing to non-uniformity in the spatial distribution of the particles. If the particles were identical in size and shape and were arranged in a perfect lattice, the powder would act like a continuous medium of index m and would transmit plane waves without scattering (unless the wavelength were short enough to allow coherent Bragg reflections). Such a plane has the usual form

$$\phi = a\, e^{-im(\vec{\kappa}_o \cdot \vec{r})} \tag{34}$$

where $\vec{r}$ is the vector position of a point in the medium, $\vec{\kappa}$ is the wave propagation vector (of magnitude $\kappa_o = 2\pi/\lambda_o$, ϕ is the field, which we consider for simplicity to be a scalar, and a is the field amplitude.

The wave is a solution of the wave equation

$$\nabla^2\phi + m^2\ \kappa_o^2\phi = 0 \tag{35}$$

The effect of nonuniformity in the spatial distribution of the particles is that m^2 is replaced by $m^2 + \Delta m^2$ where Δm^2 is the fluctuation in m^2 caused by the nonuniformity. The new wave equation can be written in the form

$$\nabla^2\phi + m^2\ \kappa_o^2\phi = -\ \kappa_o^2\Delta m^2\phi \tag{36}$$

This equation has a solution of the form

$$\phi = a\ e^{-im\vec{\kappa}_o^2\cdot\vec{r}} + \phi_s \tag{37}$$

where ϕ_s is given by

$$\phi_s = -\ \frac{1}{4\pi}\int_V \frac{e}{R}^{-im\kappa_o R}\ (\kappa_o^2\Delta m^2\phi)dV \tag{38}$$

This equation gives the scattered wave ϕ_s at some measurement point P due to the scattering that takes place in a volume V. An element dV of V is located at the point $\vec{r}$ and the distance from dV to P is R.

In order to make the integral for ϕ_s tractable, three approximations are necessary. First, we adopt the usual Born approximation in which ϕ_s is considered to be small compared with the incident wave, so that ϕ in the integrand is replaced by the plane wave expression given by Equation (34). Second, we assume that the measurement point P is so far from the volume V that

$$\frac{1}{R}\ e^{-im\kappa_o R} \approx \frac{1}{R_o}\ e^{-in\kappa_o R_o + in\vec{\kappa}_s\cdot\vec{r}} \tag{39}$$

where R_o is the distance of P from the origin of coordinates located at the center of the volume V and $\vec{\kappa}_s$ is the wave vector of the radiation scattered in the direction from the origin to P. As the third approximation we have also, for mathematical tractability, replaced m in the exponential factor by its real part n. With these three approximations the integral for ϕ_s becomes

$$\phi_s = \frac{1}{4\pi} \frac{\kappa_o^2 a}{R_o} e^{-in\kappa_o R_o} \int_V e^{-in(\vec{\kappa}_o - \vec{\kappa}_s)\vec{r}} \Delta m^2 dV \tag{40}$$

The power per steradian scattered by the volume V is

$$\frac{dW_s}{d\omega} = R_o^2 |\phi_s|^2 = \frac{\kappa_o^4 I_o}{16\pi^2} \left| \int_V e^{-in(\vec{\kappa}_o - \vec{\kappa}_s)\cdot\vec{r}} \Delta m^2 dV \right| \tag{41}$$

where I_o is the incident beam intensity (watt/cm^2).

To proceed further we must make the additional approximation of replacing Δm^2 by its real part Δn^2. This is necessary in order to relate the expression for $dW_s/d\omega$ in a reasonably simple way to the power spectral density of Δn^2 which is

$$P(\beta) = \frac{d(\Delta n^2)}{d\beta_x d\beta_y d\beta_z} = \frac{1}{8\pi^3 V} \left| \int_V e^{i\vec{\beta}\cdot\vec{r}} \Delta n^2 dV \right| \tag{42}$$

where $\vec{\beta}$ is the vector in wavenumber space complementary to $\vec{r}$. Thus we obtain the formula

$$\frac{dW_s}{d\omega} = \frac{\pi \kappa_o^4 I_o V}{2} P(\beta) \tag{43}$$

where

$$\beta = n\left|\vec{\kappa}_o - \vec{\kappa}_s\right| = 2n\kappa_o \sin\frac{\theta}{2} \tag{44}$$

Here θ is the angle between the scattered and incident beams. This relation for β is identical to the Bragg reflection condition for a set of planes of spacing $d = 2\pi/\beta$ since $n\kappa_o = 2\pi/\lambda$. The scattering $dW_s/d\omega$ in a given direction relative to the incident beam is therefore proportional to the "strength" of the Bragg planes that meet the reflection condition for that direction, i.e., to the square of the appropriate Fourier component of Δn^2.

The power density function $P(\beta)$ depends on the geometrical structure of the powder, including the degree of agglomeration of the particles as well as their shapes and size distribution. In the absence of detailed information on these matters we assume the following simple form for $P(\beta)$:

$$P(\beta) = \frac{d_e^3}{\pi^{3/2}} \left\langle (\Delta n^2)^2 \right\rangle e^{-d_e^2\beta^2} \tag{45}$$

where d_e is the autocorrelation length for Δn^2 which is of the order of the particle spacing. We will treat d_e as an adjustable parameter. The factor $d_e^3/\pi^{3/2}$ normalizes $P(\beta)$ so that

$$\int_{-\infty}^{\infty}\int_{-\infty}^{\infty}\int_{-\infty}^{\infty} P(\beta)\, d\beta_x\, d\beta_y\, d\beta_z = \left\langle (\Delta n^2)^2 \right\rangle \tag{46}$$

The symbol $\langle\ \rangle$ indicates a spatial average.

To evaluate $\left\langle (\Delta n^2)^2 \right\rangle$ we should ideally start with the Lorentz-Lorenz expression for m^2, given by Equation (11). On differencing this

expression with respect to local variations Δf_j of the f's we find

$$\Delta m^2 = \frac{1}{3} \sum_j \Delta f_j (m + 2)^2 \left(\frac{m_j - 1}{m_j^2 + 2} \right) \tag{47}$$

Therefore

$$\Delta n^2 = \frac{1}{3} \sum_j \Delta f_j \ \mathrm{Re} \left\{ (m + 2)^2 \left(\frac{m_j^2 - 1}{m_j^2 + 2} \right) \right\} \tag{48}$$

where Re stands for "real part of." The desired spatial average of $(\Delta n^2)^2$ requires that this summation be squared and then space-averaged. This would clearly result in a very complicated expression and would require sufficient knowledge of the statistical structure of the powder mixture so that all the $\langle (\Delta f_j)^2 \rangle$ and $\langle (\Delta f_j)(\Delta f_k) \rangle$ could be evaluated. Instead of undertaking so ambitious a program at this time we have simply assumed that $\langle (\Delta n^2)^2 \rangle$ is approximately the mean square difference between the local n^2 of the medium and the Lorentz-Lorenz average n^2, i.e.,

$$\langle (\Delta n^2)^2 \rangle = \sum_j f_j (n_j^2 - n^2)^2 \tag{49}$$

The scattering formula therefore becomes, from (43) and (45),

$$\frac{dW_s}{d\omega} = \frac{\kappa_o^4 I_o V d_e^3 \langle (\Delta n^2)^2 \rangle}{2\sqrt{\pi}} \ e^{-4 d_e^2 n^2 \kappa_o^2 \sin^2 \frac{\theta}{2}} \tag{50}$$

To calculate S by the six-beam method we must first apportion the scattering function $dW_s/d\omega$, resulting from an incident beam in one of the six directions, amongst the six allowed scattering directions.

We designate the powers of the scattered beams as W_f for the forward-scattered beam, W_t for the four transversely-scattered beams, and W_b for the backward-scattered beam. A suitable weighting scheme for apportioning the scattering is the following:

$$W_f = \int_0^{\pi/2} \frac{dW_s}{d\omega} \cos^2\theta \, d\omega \tag{51}$$

$$W_t = \frac{1}{4} \int_0^{\pi} \frac{dW_s}{d\omega} \sin^2\theta \, d\omega \tag{52}$$

$$W_b = \int_{\pi/2}^{\pi} \frac{dW_s}{d\omega} \cos^2\theta \, d\omega \tag{53}$$

The total backscattered power from a given forward-going beam is W_b+2W_t. Therefore

$$S = \frac{\sqrt{3}}{I_o V} (W_b + 2W_t) \tag{54}$$

where the $\sqrt{3}$ is the slant factor referred to earlier.

On carrying out the integration for W_b and W_t with $dW_s/d\omega$ given by (50), we obtain for the backscattering coefficient:

$$S = \frac{\sqrt{3\pi}}{4} \frac{\langle (\Delta n^2)^2 \rangle}{n^4 d_e} G(x) \tag{55}$$

$$\text{where} \quad x = 2\pi n d_e / \lambda_o \tag{56}$$

and

$$G(x) = \frac{2x^2 - 1 + 2e^{-2x^2} - (1 + 2x^2 + 4x^4)e^{-4x^2}}{2x^2} \qquad (57)$$

The function G(x) varies as x^4 for small x and approaches 1 for large x.

An alternative way of determing S, which is analogous to the calculation of the Rayleigh scattering of a gas in terms of the incoherent scattering of the individual molecules, is by means of the "immersed particle" model. Here we regard a given particle of index n_j as though it were immersed in a medium of index n, the real part of the Lorentz-Lorenz index. Under these conditions it is a well-known result of electrostatics that, for a spherical particle of radius a_j, an electric field E in the medium induces in the particle a dipole moment of magnitude

$$M = \frac{4\, a_j^3\, n^2 (n_j^2 - n^2) E}{(n_j^2 + 2n^2)} \qquad (58)$$

If the electric field is produced by an incident wave of long wavelength, the total scattered power is given by

$$W_s = \frac{\kappa^3 \omega}{12\pi n^2} M^2 \qquad (59)$$

while the incident power density is

$$I_o = \frac{1}{2} E^2 \frac{\omega n^2}{\kappa} \qquad (60)$$

Here $\kappa = 2\pi n/\lambda_o$ and ω is the angular frequency of the radiation. From (58), (59), and (60) the backscattering cross-section σ_j of the particle is

$$\sigma_j = \frac{1}{2}\frac{W_s}{I_o} = \frac{4\pi}{3}\kappa^4 a_j^6 \left(\frac{n_j^2 - n^2}{n_j^2 + 2n^2}\right)^2 \qquad (61)$$

The total backscattering coefficient is

$$S = \sqrt{3}\sum_j \frac{f_j \sigma_j}{v_j} = \sqrt{3}\,\kappa^4 \sum_j f_j a_j^3 \left(\frac{n_j^2 - n^2}{n_j^2 + 2n^2}\right)^2 \qquad (62)$$

where v_j is the volume of the (spherical) particles of type j.

3. Formula for R_v and Criterion for Selecting Fine- or Coarse-Particle Model

To determine the volume reflectance, on either the coarse- or the fine-particle model, we insert the calculated values of S and K in the previously mentioned Kubelka-Munk formula:

$$R_v = 1 + \frac{K}{S} - \sqrt{\frac{K^2}{S^2} + 2\frac{K}{S}} \qquad (2)$$

Which model we use at a given wavelength depends on suitable criterion for the limit of validity of the fine-particle model. The criterion that we have adopted is that the value of S calculated by the fine-particle theory should not exceed a critical value S_o determined by the sum of the physical cross-sections of all particles in a unit of volume.

It is true that, according to the Mie theory, the total scattering cross-section σ of a single particle can exceed the physical cross-section σ_o at certain wavelengths owing to resonance within the particle. However, in a powder of closely-spaced interacting particles

having a substantial spread in effective diameter, this effect is largely averaged out. The effect of diffraction, which also contributes significantly to the total cross-section in the Mie theory, does not have to be separately considered since it is included in both our Bragg reflection and immersed-particle models.

The magnitude of S_o is given by

$$S_o = \frac{1}{2} \sum_j \frac{f_j}{v_j} \sigma_{o,j} \tag{63}$$

where $\sigma_{o,j}$ and v_j are the average physical cross-section and volume respectively, of particles of type j. The factor of 1/2 allows for the backscattered part of the total scattering. In applying criterion (63) we switch from the fine-particle to the coarse-particle model whenever the fine-particle value of S greatly exceeds S_o. The changeover takes place for both the surface and the volume reflection.

D. OVERALL REFLECTANCE R

The overall reflectance R of the powder includes the effects of R_e, R_i, R_v and also the effect of diffusion of the incident collimated beam.

The intensity I_c of the incident collimated beam decays owing to both scattering and absorption according to the differential equation

$$\frac{dI_c}{dx} = -\frac{1}{2}(2S + K)I_c \tag{64}$$

where the 1/2 allows for the shorter distance traveled by collimated than diffuse radiation. The factor of 2 multiplying S allows for the fact that forward and back scattering reduce the strength of I_c equally, on the assumption of isotropic scattering. The solution of the differ-

ential equation is

$$I_c = (1 - R_e)I_o\, e^{-\beta x} \tag{65}$$

where I_o is the intensity of the incident beam and β is the extinction coefficient of the beam, given by

$$\beta = S + \frac{1}{2} K \tag{66}$$

The factor $1-R_e$ allows for the loss due to external reflection.

The radiation scattered out of the collimated beam acts as a distributed source of diffuse radiation. On inserting this source as an additional term in the usual Kubelka-Munk differential equations we solve these equations for the distribution of diffuse radiation in the powder (see Appendix). On applying the surface boundary conditions to the diffuse radiation we finally arrive at the formula already cited for the overall reflectance:

$$R = R_e + \frac{(1 - R_e)(1 - R_i)R_v}{(1 - R_i R_v)} \left(\frac{2}{3 - R_v}\right) \tag{1}$$

The reflectance for diffuse incidence is given by the same expression with the omission of the last factor, $2/(3-R_v)$. When R_v is near 1 the collimation factor is also near 1 and the effect of collimation is small. This is to be expected since high R_v means high S/K and therefore rapid diffusion of the collimated beam. When R_v is small the collimation factor approaches its minimum value of 2/3.

III. PROGRAMMING THE THEORY

The theoretical treatment given in the preceding section has grown and evolved continually for several years. A flexible set of computer programs has been written mostly in FORTRAN IV so that the predictions of the theory could be compared with experiment. The usefulness of a computer in the development of this theory is very evident when one attempts to carry out the calculations involved with a desk calculator, for instance. At any spectral frequency a typical calculation of the reflectance is a matter of hours and the incidence of errors is, of course, high. The real difficulty, however, is that a calculation at a single frequency is next to useless as the real information desired is the shape of the spectrum. The very complex behavior of the input optical constants[16,17] throughout the interesting spectral region (both n and k can vary by three orders of magnitude over a small spectral region) results in rather different behavior at nearly adjacent frequencies. Bands may tend to shift one way or another and meaningful trends are only apparent when one examines the spectrum. The richness of information inherent in the optical constants is, of course, the factor that gives infrared spectroscopy its uniqueness. In order to fully examine a spectrum, we typically make the calculations at 450 points. Yet the computer times for a given mixture (three components including vacuum) run around one minute if both coarse-particle and fine-particle theories are run together. This includes generation of the optical constants at each frequency from a table of dispersion parameters as will be discussed below. No real attempt has been made to optimize the computer times and considerable savings are undoubtedly possible.

The main computations have been carried out on an IBM 7094. A printed output is obtained and a tape is produced. The tape is used to produce plots of the data using our IBM 360/40 computer and a Calcomp plotter. The plots are invaluable as discussed above and save considerable effort due to the large number of frequencies at which the calculations are performed.

These programs necessarily have a large hierarchy of I/O paraphernalia and as we frequently have wanted to test ideas at a small number of frequercies, we have made use of a time-sharing computer system operated through remote teletypes by the General Electric Company. This system is ideal for rapid debugging and uses a large (GE 235) computer. The system limitations are principally I/O but it serves as a very useful adjunct in our work.

The basic scheme of our computer calculations is as follows. An initial data card specifies the frequency limits and the frequency increment at which the calculations are to be made. It also specifies the number of mixtures to be examined and whether the coarse-particle theory or the fine-particle theory, or both, is to be used. Various possible options for using the program are obtained by multiple entries into the main housekeeping program. The data to be used consists of a set of approximately 20 classical oscillator parameters for each material. These values had been obtained by curve fitting of the classical oscillator equations to measured data.[16,17] They are values for the high frequency dielectric constant ε_∞; and ν_i the frequency, ρ_i the strength, and γ_i the width of each oscillator present. They are the parameters of the classical oscillator dispersion equations:

$$n^2 - k^2 = \varepsilon_\infty + \sum_i 4\pi\rho_i\nu_i^2 \frac{\nu_i^2 - \nu^2}{(\nu_i^2 - \nu^2)^2} + \gamma_i^2\nu^2\nu_i^2 \tag{67}$$

$$nk = \sum_i 2\pi\rho_i\nu_i^2 \frac{\gamma_i\nu\nu_i}{(\nu_i^2 - \nu^2)^2 + \gamma_i^2\nu^2\nu_i^2} \tag{68}$$

The optical constants are calculated from these equations at each frequency. This procedure saves considerable computer storage space as large tables of n and k are unnecessary. These values together with the input volume fractions and particle sizes are then used in the subsequent calculations. When the General Electric remote console system is used,

values of n and k are read from tables that the 7094 program produces so as to eliminate these computations. The subroutines that compute the fine-particle and coarse-particle reflectances also produce R_e, R_i, R_v, K and S and a host of other intermediate results. All of these can easily be monitored in order to trace the important effects of changes in the input parameters. We thereby have a useful method of gaining considerable insight into what is often a very complicated interaction of effects.

IV. EXPERIMENTAL PROGRAM

The spectra of powders under unfavorable circumstances, such as very fine-particle size and high porosity, tend to show low reflectances or nearly blackbody conditions.[3,7] The compositional information while still present may be observed only with great difficulty owing to an insufficient signal-to-noise ratio. Further, the spectral emission under ambient conditions is rather weak. Under conditions of remote observation, such as from an orbiting space vehicle, the area under observation can only be observed for a limited time depending on the orbital speed, height, etc. Observations through part or all of the earth's atmosphere or through planetary atmospheres contain considerable interferences. For all of these reasons, reliable experimental observations require the highest possible signal-to-noise ratio in the spectrum. In order to decipher the possibly very complex spectrum of a mixture of rocks and powdered minerals, it would be best to conduct a very broad-band experiment. These factors have led us to propose[1,18] that the optimum remote sensing infrared spectrometer would be a Michelson interferometer.

A. FOURIER SPECTROSCOPY

The technique of Fourier spectroscopy has received much attention in recent years. This is not the place for a substantive discussion of this technique as there are a number of excellent discussions in the literature.[19-21] However, a brief description will be useful.

A schematic diagram of a Michelson interferometer is given in Figure 1. A monochromatic beam of radiation is divided into two beams at the partially reflecting, partially transmitting beam splitter. One of these beams travels to a fixed mirror and the other to a movable mirror. The beams are recombined at the beam splitter and part of the recombined beam then falls on the detector. When the path difference for the two beams is zero, constructive interference results. However,

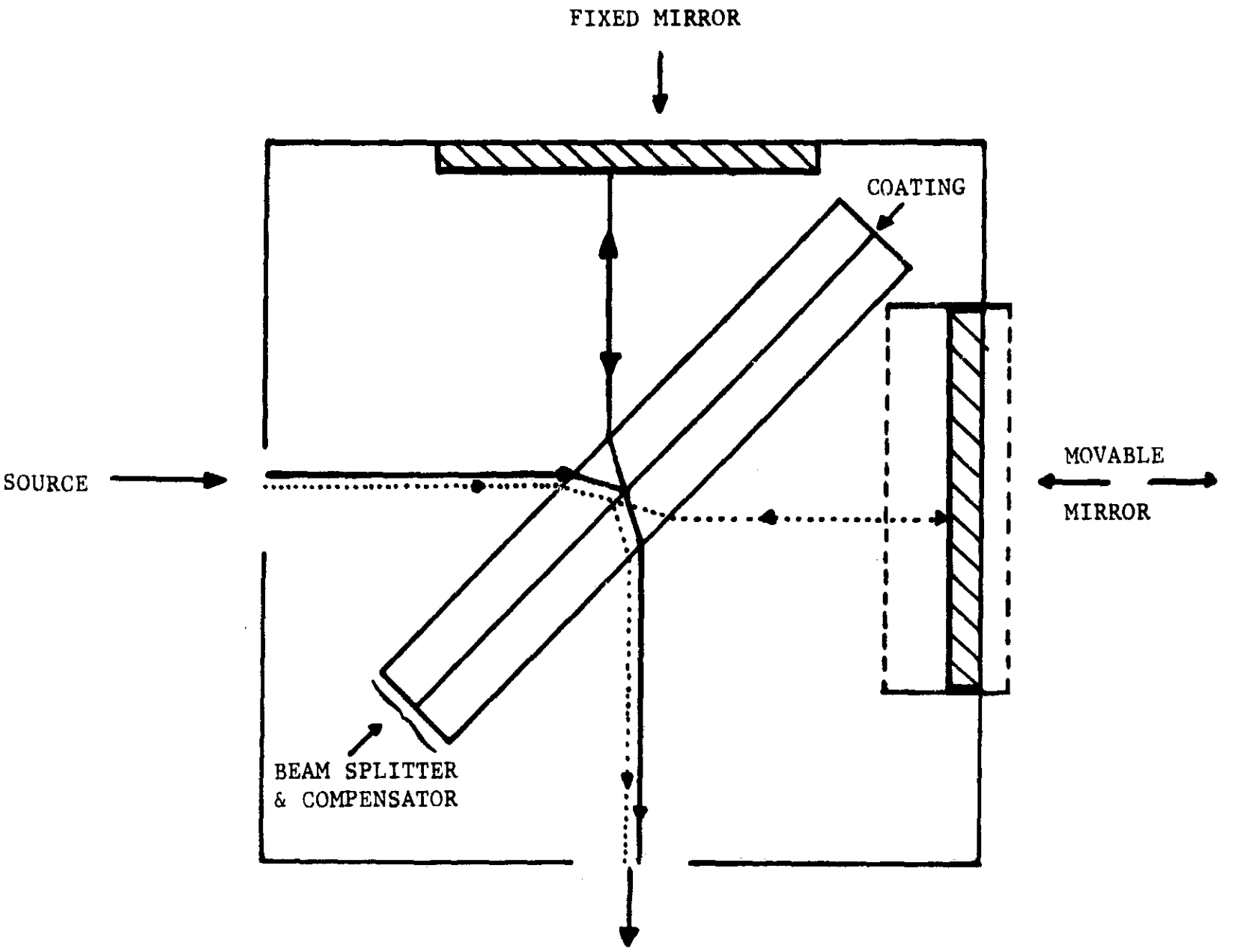

FIGURE 1. SCHEMATIC DIAGRAM OF MICHELSON INTERFEROMETER CUBE

at path differences not equal to an integral number of wavelengths the interference is more or less destructive. Thus a sinusoidal intensity fluctuation is recorded by the detector with a period set by the radiation wavelength and velocity of movable mirror travel. For polychromatic radiation this takes place for every wavelength and the result is a trace, such as shown in Figure 2, called an interferogram. This interferogram contains information as to all the wavelengths present at the detector, each being encoded by its wavelength and the mirror velocity. Fourier spectroscopy is the technique of decoding this interferogram by means of a Fourier transformation. The basic equations of Fourier spectroscopy are:

$$I(x) = \int_{-\infty}^{\infty} B(\nu) \cos 2\pi\nu x \, d\nu \tag{69}$$

$$B(\nu) = \int_{-\infty}^{\infty} I(x) \cos 2\pi\nu x \, dx \tag{70}$$

where $B(\nu)$ represents the spectrum at the frequencies ν and $I(x)$ represents the interferogram as a function of path difference x. The revival of interest in the interferometer as a spectrometer dates from the early 1950s when several inherent advantages of Fourier spectroscopy over conventional prism and grating techniques were recognized. The first advantage is the so-called Fellgett[22] or multiplex gain in signal to noise. The idea is that because all frequencies are examined simultaneously rather than sequentially the radiation is not being wasted on the slit jaw as in a dispersion spectrometer. For otherwise identical systems this leads to a signal-to-noise gain proportional to $\sqrt{N}$ where N is the number of resolution elements. The other principal advantage is usually called the throughput advantage. While this has some subtleties, it can be basically viewed as resulting from a different relationship between spectral resolution and energy throughput than

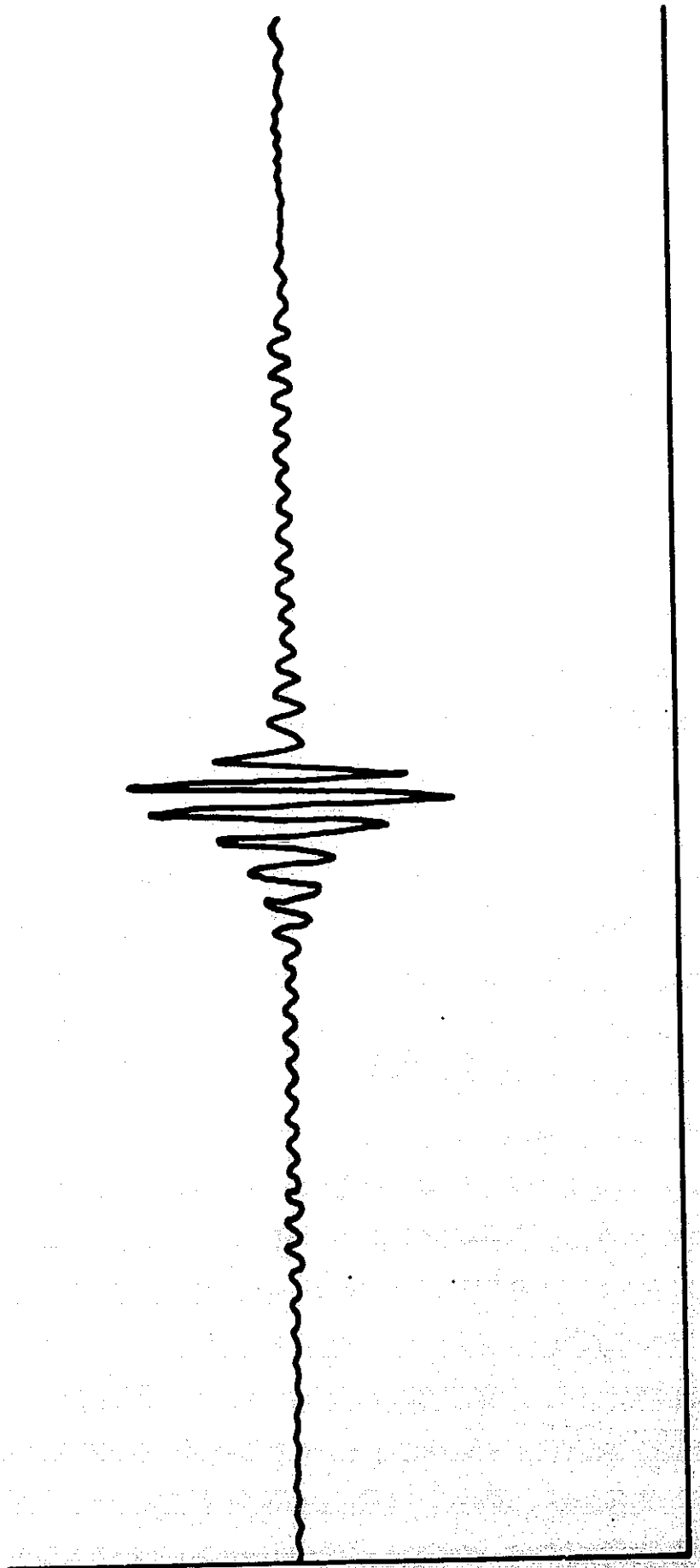

FIGURE 2. TYPICAL INTERFEROGRAM

occurs in a dispersion spectrometer. For a conventional spectrometer an increase of a factor of two in resolution is accomplished by halving the slit width. As spectrometers utilize both entrance and exit slits which should be operated together, the energy throughput is thereby decreased by the square of the slit width, a factor of four. For the interferometer however, there is no slit. A single aperture takes its place. The resolution in this instrument depends principally on the travel distance of the movable mirror. Thus within reason a quite large aperture may be used resulting in large energy throughput without seriously degrading the resolution. Ultimately, the phase shifts of oblique rays limit the allowable aperture, but for viewing extended sources and under comparable other conditions the throughput advantage can be of the order of a factor of 100.[23] In general, interferometers tend to be compact relatively light weight instruments but in order to utilize the method of Fourier spectroscopy rather sophisticated data acquisition and computing equipment is required. Indeed, it is quite apparent that the renaissance of Fourier spectroscopy is largely due to the tremendous advances in digital computers and computer techniques. Despite these factors, interference spectroscopy has lagged in development for a number of reasons. First, the mathematical sophistication and computer programming abilities necessary are formidable obstacles. The interferogram provides little insight into spectral results until after Fourier transformation which usually requires some elapsed time. Electronic wave analyzers are available but they suffer some defects in that phase information is lost. The lack of general demand for interferometers and relatively recent generally availability of computers has resulted in slower development of interferometers than of comparable dispersion spectrometers. The mechanical requirements for the drive are critical and much effort has been spent in this area.

B. OUR INSTRUMENTATION

The great advantages of Fourier spectroscopy over conventional dispersion techniques for obtaining the emittance spectra of relatively

weak extended sources over a wide band of frequencies led us to delve into this technique, despite the complexity of operation. Our first experience with these instruments is detailed in a recent paper.[5] We were able to obtain emittance spectra of a series of well sized corundum powders using a Block Model 195C interferometer spectrometer having a spectral resolution of about 15 cm^{-1}.

We purchased an Idealab IF 3 interferometer and Hewlett-Packard 2116B computer-based digital data acquisition system for use on this project. The interferometer is shown in Figure 3 and the overall system in Figure 4. The interferometer has three channels. There are channels with separate detectors above and below the infrared channel for a "white" light and a helium neon laser. The laser is used to specify the sampling times. The interferogram of the laser light is a sine wave, the zero crossings of which are used as sampling positions. Thus drive imperfections are effectively monitored. The frequency of the laser (15803 cm^{-1}) is significantly higher than any frequency of interest in the main channel in order that the requirements of the sampling theorem be satisfied. The "white" light produces an interferogram that has a relatively sharp central maximum. It is used to flag a particular laser zero crossing so that successive interferograms can be coherently added. It is thus possible to improve the signal-to-noise ratio by adding a number of separate runs together. The white light channel fixed mirror is offset from the main mirror by about 0.5 mm. This produces a signal that we take as the start of a run. The interferometer can be operated at 10 different resolutions ranging from 10 cm^{-1} to 1 cm^{-1} (corresponding to optical path differences of 1 mm to 1 cm) and at velocities ranging from 1 mm/min to 4 mm/sec. Greater speeds are also available but they would require different detectors.

The main channel detector is a 5 mm by 5 mm Barnes Engineering Company pyroelectric detector made of triglycine sulfate. This is a thermal detector that "acts like a capacitor with a temperature-dependent charge buildup. As the incident radiation is absorbed, the

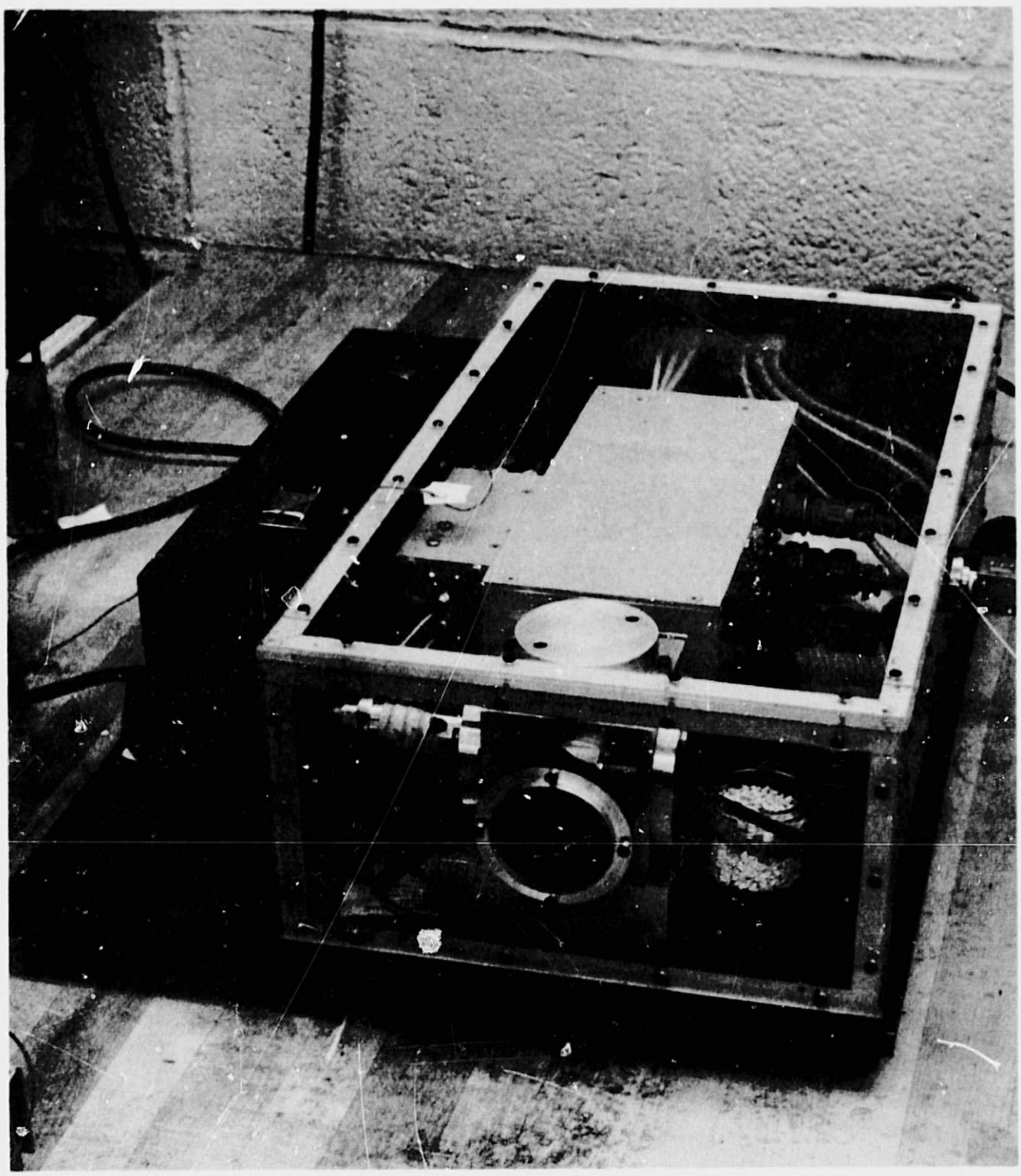

FIGURE 3. INTERFEROMETER

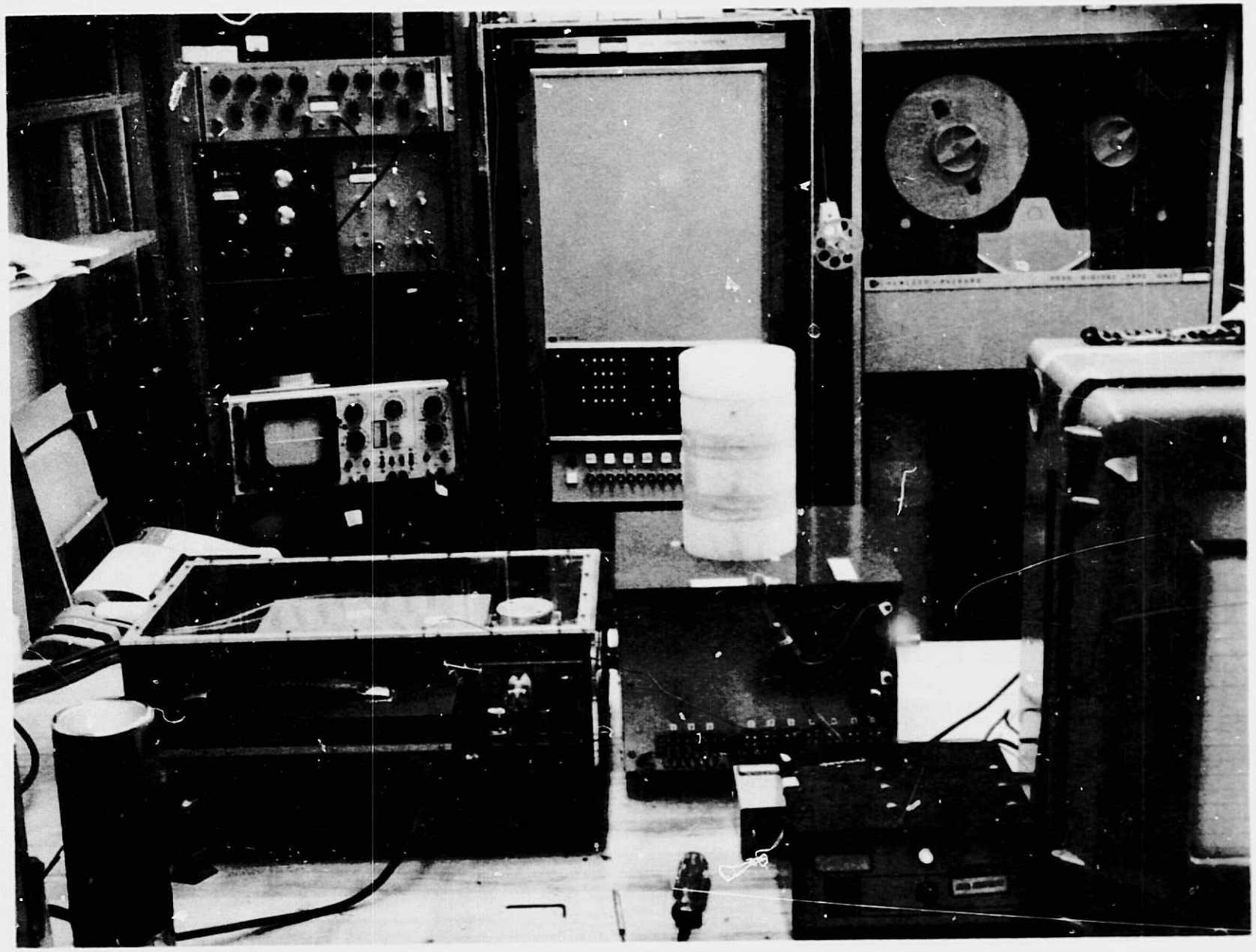

FIGURE 4. INTERFEROMETER SYSTEM

temperature of the detector changes. This, in turn, changes the charge and resultant voltage."[24] We chose this detector, which has a similar D* to a thermistor bolometer, because it can be operated down to d-c. This is very important as it permits us to use the slow scanning speeds of the interferometer without external chopping.† Another reason for choosing this detector is that it can be obtained in physically large sizes. The importance of the physical size of the detector can be seen when one recognizes that the radiation to be detected is that reaching the center of the equal inclination (Haidinger) fringe pattern. This radiation is modulated by the changing path difference for each wavelength present. However, the modulation is decreased if too large a detector size is utilized owing to partial cancellation of bright and dark fringes. The resolution of the instrument is controlled by the movable mirror travel, and this together with the aperture size establishes the useful size of the detector.[19] To put it another way, if one wishes the maximum throughput for a given resolution, the aperture of the instrument is matched to the detector size and the speed of a KRS 5 lens that focusses the radiation on the detector. The effective detector size

$$D = 2f \frac{\lambda}{2X} \tag{71}$$

where D is the linear dimension of the detector, λ is the wavelength corresponding to the central frequency of the band or interest, f is the focal length of the KRS 5 lens, and 2X is the optical path difference. This represents a compromise in the acceptable size of the central spot of the Haidinger fringe pattern among the various frequencies of interest. Actually, in order to take account of diffraction by the lens, 0.6 D is used[25] instead of D. For higher resolutions the greater path differences will reduce the permissible size of the detector. We therefore have a

---

†The literature on this detector[24] claims a frequency response from d-c to beyond 10 KC so we felt this detector might also be utilized at high scan speeds.

series of aperture plates which can be attached to the detector housing to match the detector size required.

One disadvantage of this detector is that it must be kept below its Curie point which is 48°C. This corresponds to a flux of more than 0.1 watts/cm^2. Thus very hot sources must not be focussed on the detector.

The instrument has two interchangeable beamsplitters. The first is made of calcium fluoride coated with silicon and has an intended range of operation of 2-9 microns. It has proved particularly useful in our initial interferometer testing as it is relatively rugged and insensitive to atmospheric humidity. The second beamsplitter is cesium iodide, coated with germanium with a range of operation of 8-40 microns. The coating thickness is chosen to establish the spectral range of operation by setting the characteristics of the interference modulation resulting from the film thickness (channel spectrum). As the optical quality of CsI is significantly less than that of CaF_2, the beamsplitter sections pertaining to the laser and white-light channels are made of CaF_2.

The entire cube and transducer mechanism are mounted on an aluminum block and enclosed by a lucite box with a KRS 5 entrance window. This box is intended to be flushed with dry nitrogen to protect the moisture-sensitive CsI beamsplitter. It also insulates the interferometer from thermal gradients in the room. We have chosen to monitor the temperature of the interferometer rather than control it at the present time.

C. PROGRAMMING THE INTERFEROMETER SYSTEM

In order to obtain meaningful spectra from the interferometer, three computer programs were written, one for the Hewlett-Packard 2116B computer and two for the IBM 360. The function of the Hewlett-Packard

program is to sample the output signal from the interferometer at appropriate intervals, preprocess the resulting interferograms and write them along with other relevant parameters on a tape in a form suitable for processing by the IBM 360.

At the beginning of a run the computer requests the operator to supply it with information on the scan speed, the required resolution, the interval at which a sample is to be taken, the mode of collection, and the number of coherent additions of interferograms desired. It computes storage requirements and, if adequate storage is available, it instructs the operator to proceed with the run.

Two modes of collection are available--a skip mode and a totaling mode. For the skip mode a data sample is taken at laser fringe intervals specified by a parameter called the group size. In the totaling mode, a sample is taken at each laser fringe and the sum of the values over a group of fringes are added together and stored as a single data point. The totaling mode is essentially a low pass filter to further attenuate those high frequencies passed by a Krohnhite electronic filter. The highest frequencies of interest in the calculated spectrum are also attenuated somewhat. For example, the amplitude of the frequency component that is two thirds of the Nyquist folding frequency is attenuated to 80% of the value that would be obtained by the skip mode if sufficient co-additions were used to result in the same effective measurement time. The use of the totaling mode results in higher signal levels, thereby discriminating against digitizing noise. Successive scans are co-added until the specified number are collected. Data are only collected on the "outward" sweep of the mirror, but as the instrument is set to "flyback" at high velocity, little measurement time is wasted.

At the end of the data collection, the interferogram is displayed on an XY oscilloscope so that the operator can determine visually whether the interferogram should be saved for further processing, whether more co-additions are necessary, or whether the run should be discarded.

The next part of the processing consists of reducing the raw interferograms to "single beam" spectra and creating a tape file which can be used for later computation of "double beam" spectra. Processing may be roughtly divided into three stages--preprocessing of the interferogram, calculation of phase correction terms, and calculation of corrected spectra.

The preprocessing consists of truncating the left side of the interferogram so that it contains no more than 10% of the points on the right side, and filling out the right-hand side of the interferogram with zeros so that the total number of data points is an integral multiple of two.

In order to make the phase correction, a low resolution spectrum is calculated by multiplying the interferogram by a triangular apodization function extending from 10 points before the central maximum to 10 points beyond it. Apodization (literally, removing the feet),[19] refers to the fact that the Fourier transform, strictly speaking, requires the use of an integral extending over an infinite range of path differences. As this is of course impossible, the finite limits actually used introduce spurious side bands onto spectral features. These side bands may be attenuated by the use of an appropriate weighting or apodization function when constructing the integral.[19] Subsequent Fourier transformation results in a low resolution spectrum whose phase angle can be used to remove any effects of uncertainty in the position of the central maximum as well as mild chirping[21] following the scheme of Mertz.[26]

The final stage of processing consists of multiplying the original interferogram by a trapezoidal apodization function which is zero at the first point of the interferogram and increases linearly to a maximum value of unity at a distance on the right-hand side of the central maximum equal to the distance from the starting value to the central maximum. The apodization function remains at unity halfway to

the end of the nonzero portion of the interferogram and then decreases linearly to zero at the last point on the interferogram. This apodized interferogram is then transformed using the Cooley-Tukey algorithm[27] and the modulus is multiplied by the cosine of the difference between the phase angle obtained with the initial short apodization function and that obtained with the trapezoidal apodization function just described, to yield the final finished spectrum. This spectrum is then saved on the tape file and can be displayed on the Calcomp plotter.

The third and final part of the processing consists of comparing sample and background spectra from the tape file and computing double beam transmission, reflection, or emission spectra for the sample. The selection of the pairs of spectra to be processed and the choice of transmission, reflection, emission, or single beam spectra to be plotted is specified on control cards read in at execution time. The facility to recognize and handle aliased spectra and to plot the principal alias in the proper frequency range is also incorporated in our computer programs.

D. TEST RUNS

The nature of our intended experimental program has a number of subtle features (vide infra.). Because we have a relatively short acquaintance with Fourier spectroscopy, we chose therefore to write our software and establish the methods of using the interferometer under conditions where our techniques could be checked out against known spectra. A number of thin-film transmission and blackbody emission runs were made in both the CaF_2 and CsI regions under varying resolutions. The films used were polystyrene and polyethylene. The blackbody was a large aluminum block having milled V-grooves which were sprayed with 3M black paint. This blackbody is believed to have a spectral emittance of 0.99 throughout the region of interest. Figure 5 is a spectrum of a polystyrene film obtained during the interferometer check-out period in the region of the CaF_2 beamsplitter.

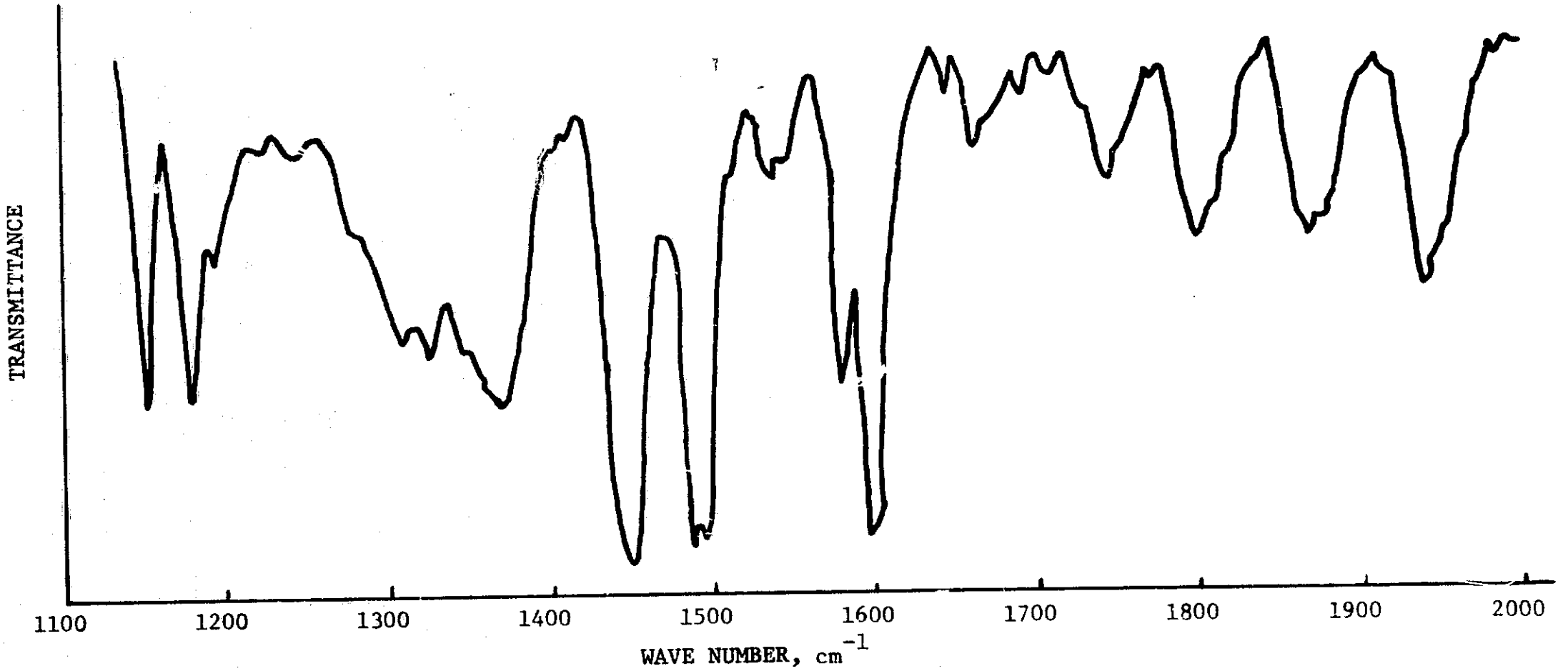

FIGURE 5. TRANSMITTANCE OF POLYSTYRENE

E. EMITTANCE SPECTRA OF POWDERS

In any remote infrared spectroscopic experiment for the moon, Mars, or the earth during the daytime, the quantity measured would be the emittance rather than reflectance at wavelengths beyond about 4 microns. Of course, at night only the emittance is measurable. While we have shown experimentally that Kirchhoff's law is valid for powders[5] we decided that our experiments would more closely approximate the remote sensing experiments that we desire to see performed if we measured emittance directly. The great bulk of the compositional information for minerals lies beyond 4 microns. The only significant infrared mineral bands that occur short of 4 microns are those due to water, either bound or free, and the ferrous ion electronic band. The latter has been used with some success in remote sensing experiments[28,29] but it is not a truly mineralogical diagnostic.

The purpose of the experimental program is to carry out sufficient critical experiments to establish the effects of changes in the various parameters on the spectra of natural surfaces and thus to guide the development of the theory. We believe the parameters of the spectral reflectance or emittance function are the radiation wavelength λ, the wavelength dependent refractive index n and absorption index k, a measure of the particle size d, and the volume fraction f for each component present. The components of the mixture include vacuum, having n=1, k=0, and a volume fraction equal to the porosity of the medium.

F. SAMPLE POWDERS

We have chosen to carry out our experiments principally on corundum and quartz powders. The optical constants for both materials are well known[16,17] and in a convenient form for our computer calculations as discussed previously. Corundum is a grinding material and so is available in known rather narrow particle size distributions. After a number of inquiries we obtained a set of well sized (Figure 6) samples

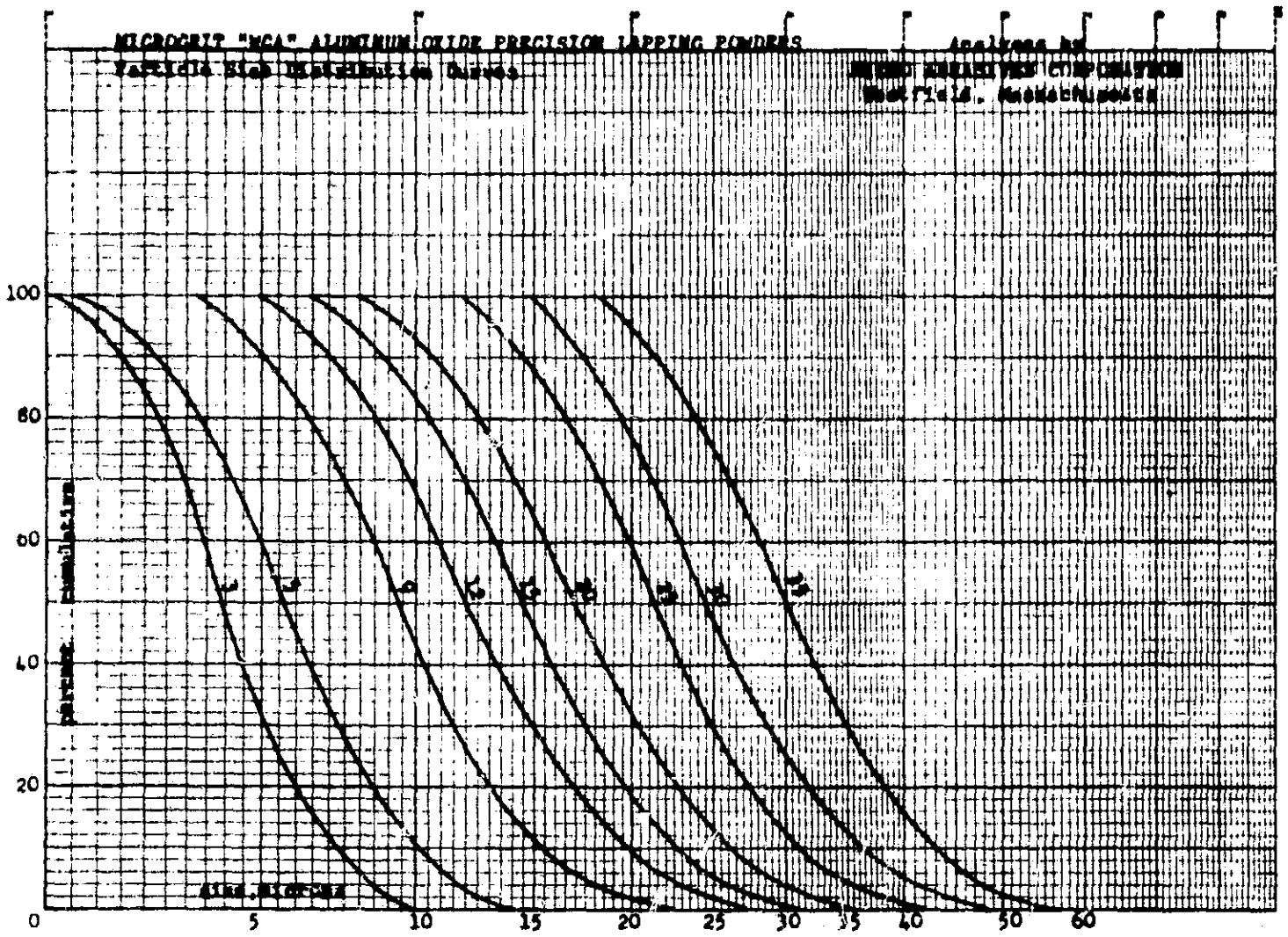

FIGURE 6. CORUNDUM PARTICLE-SIZE DISTRIBUTIONS

of α-Al_2O_3 (Microgrit "WCA" aluminum oxide precision lapping powders) from the Microabrasives Corporation of Westfield, Massachusetts. The manufacturer states[30] that each particle is a discrete crystal and has a purity of over 99%. The crystals have a platelet shape with their thickness averaging about 1/5 of their diameter. The c-axis is perpendicular to the platelet face. These samples were placed in a flat pan-shaped container of sufficient depth to insure that no radiation directly from the pan would be measured, and the edge of a spatula was run across the top surface. A similar preparation was used to obtain scanning electron micrographs of these surfaces. Figure 7 shows the nature of the surfaces. These micrographs were obtained using a secondary electron image made with a JSM-2 Scanning Electron Microscope by the courtesy of Mr. G. Goswell, Dr. J. Russ, and Mr. A. Kabaya of JEOLCO, U.S.A., Inc. Further details are given in our previous paper.[5]

An obvious difficulty with using this material for theoretical modeling is caused by the platelet shape. It appears that the orientations of the crystallites are not completely random, as some plates tend to stack. Because the optical constants are a function of orientation, we were in some doubt as to the best method of theoretically apportioning the volume fractions of the two orientations for which spectra are available. Our choices are discussed below.

A somewhat better sample geometry should be afforded by quartz powder. Quartz tends to fracture conchoidally so that this hexagonal crystal powder can be considered to be made up of a 2:1 ratio of particles having the electric vector aligned perpendicular and parallel to the c-axis, respectively. We will discuss data obtained for quartz powder by ourselves,[1] and the National Bureau of Standards[31] below. A scanning electron micrograph of one of the NBS samples is shown in Figure 8. This was taken on our new Cambridge Instrument Company Stereoscan II scanning electron microscope by essentially the same techniques as previously discussed.[5] The poor quality of this picture is due to difficulty in coating the quartz. It is clear from this photograph that the nominal

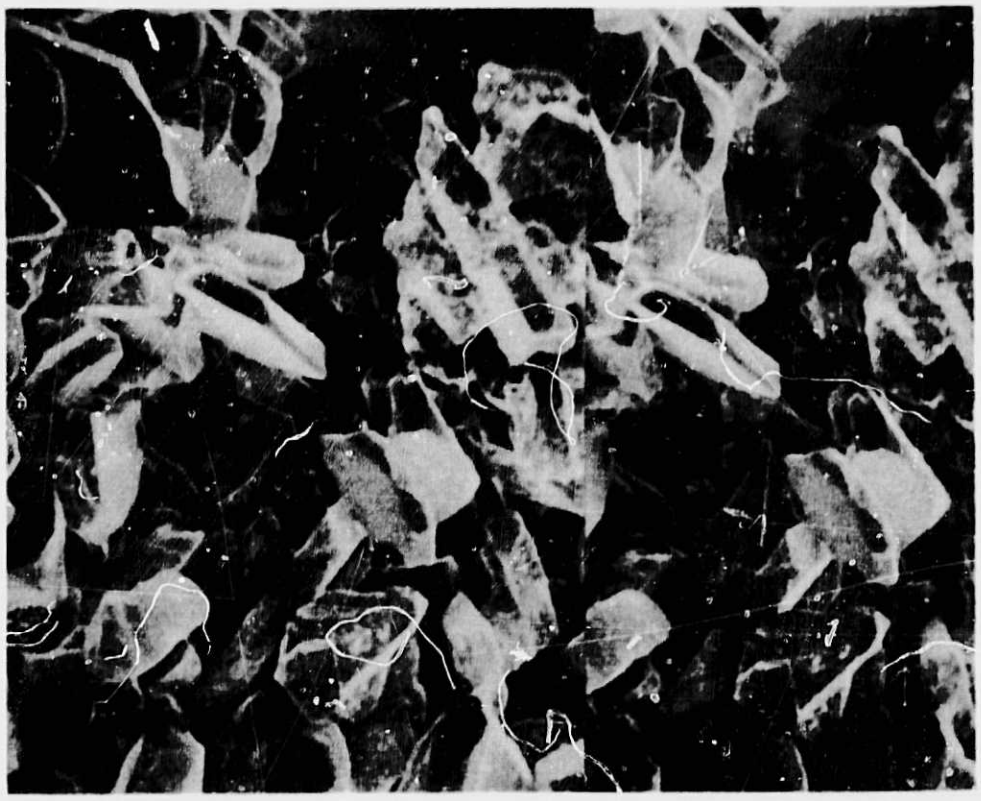

FIGURE 7. CORUNDUM POWDER SURFACE (15 WCA) STEREO PAIR MADE WITH JSM-2 SCANNING ELECTRON MICROSCOPE (1500X)

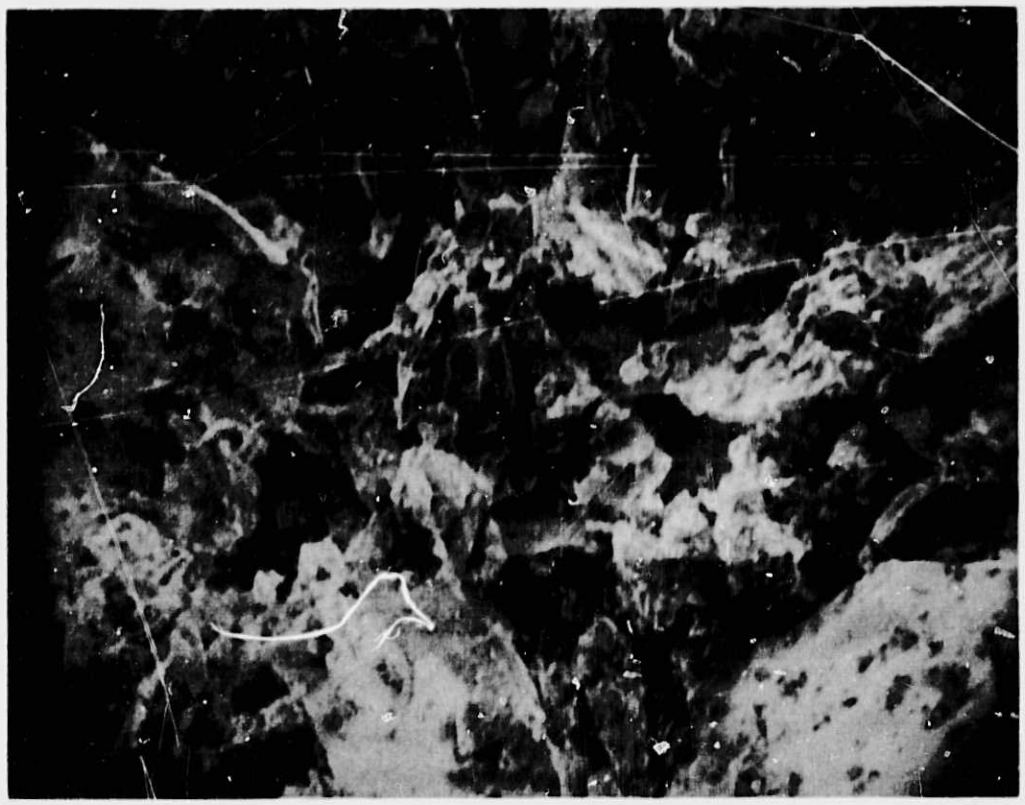

FIGURE 8. QUARTZ POWDER SURFACE 500X
(NOMINAL 63 μ > d > 53 μ)

particle size is an unrealistic representation of these samples. The samples were obtained by screening techniques and many small particles evidently adhered to the larger particles.

G. EXPERIMENTAL MEASUREMENTS

In order to measure the emission from a sample, it is important that there be a temperature difference between the sample and the background. Otherwise, the emittance of the sample is masked by its reflectance of background radiation. The measured radiance at any wavelength is essentially

$$N = \varepsilon_s B(T_s) + R_s B(T_b) \tag{72}$$

where ε_s is the emittance of the sample, R_s is its reflectance, B is the blackbody function, and T is the absolute temperature. A more precise treatment is given in the next section. When the temperature of the sample and background are equal, Kirchhoff's law

$$R_s = 1 - \varepsilon_s \tag{73}$$

shows that

$$N = B(T_s) \tag{74}$$

We have chosen to record the spectra of minerals as close to room temperature as possible in order to simulate expected remote sensing experiments. Therefore we decided to cool the background. Cooling of the background reduces the reflected component of Equation (72). Our first experiments of this sort were carried out in a copper enclosure cooled by dry ice.[5] We used a Block Engineering Model 195 TC interferometer spectrometer and measured a series of well sized corundum powders. These data were reduced for us by Mr. I. Coleman of Block Engineering, using

a slightly different scheme than discussed below. The experimental details have been described previously[5] and the most important data are summarized in Figure 9. The sample chamber was flushed with dry nitrogen, but, unfortunately, the calibration experiment showed some residual CO_2 and H_2O absorption. These resulted in the apparent emission peak at 667 cm^{-1} (CO_2) and other apparent emission peaks due to water vapor (near 575 cm^{-1} and beyond about 1200 cm^{-1}). As we only had a limited time with the interferometer, we were unable to repeat these experiments. (The interferometer was loaned to us through the courtesy of Block Engineering Company.)

These emittance results corresponded very well to data obtained by dispersion spectroscopy at the National Bureau of Standards[32] for the reflectance of the same materials. Figures 10, 11, and 12 show the comparison which we feel provides an experimental validation of the applicability of Kirchhoff's law to powders. Figure 13 shows in greater detail the very interesting spectral variations with particle size that occur in the vicinity of 500 cm^{-1}. At frequencies less than 1000 cm^{-1} the rest of the dependence of these spectra on particle size is apparently monotonic. As can be observed from Figure 10 this is not true at frequencies greater than 1000 cm^{-1}.

The experimental enclosure (Figure 14) for measuring the emittance of powders with our new interferometer is analogous to that used with the Block instrument.[5,33] In order to avoid calibration problems, such as we encountered there, we decided to mount both the sample holder and a blackbody source on a lazy susan in the bottom of a styrofoam-lined box so as to preserve viewing conditions between sample and background. Because the Idealab interferometer cannot be tipped more than a few degrees a front surface mirror inclined at 45° directs radiation from either the sample or the reference blackbody into the (horizontal) interferometer through an aperture in the side of the box while a cold, black aluminum shield covers both the lazy susan and mirror. The shield is

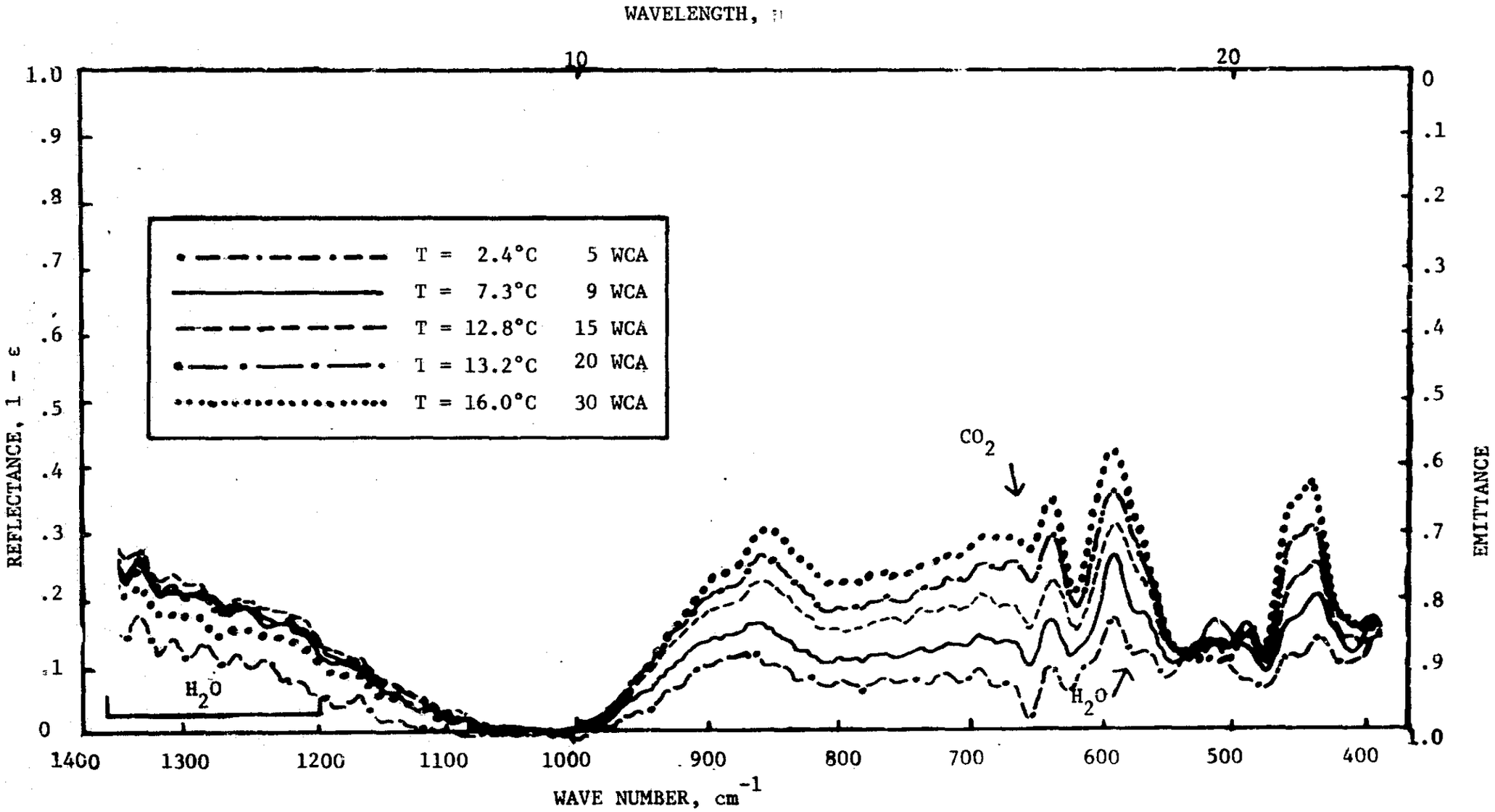

FIGURE 9. EMITTANCE SPECTRA OF CORUNDUM POWDERS

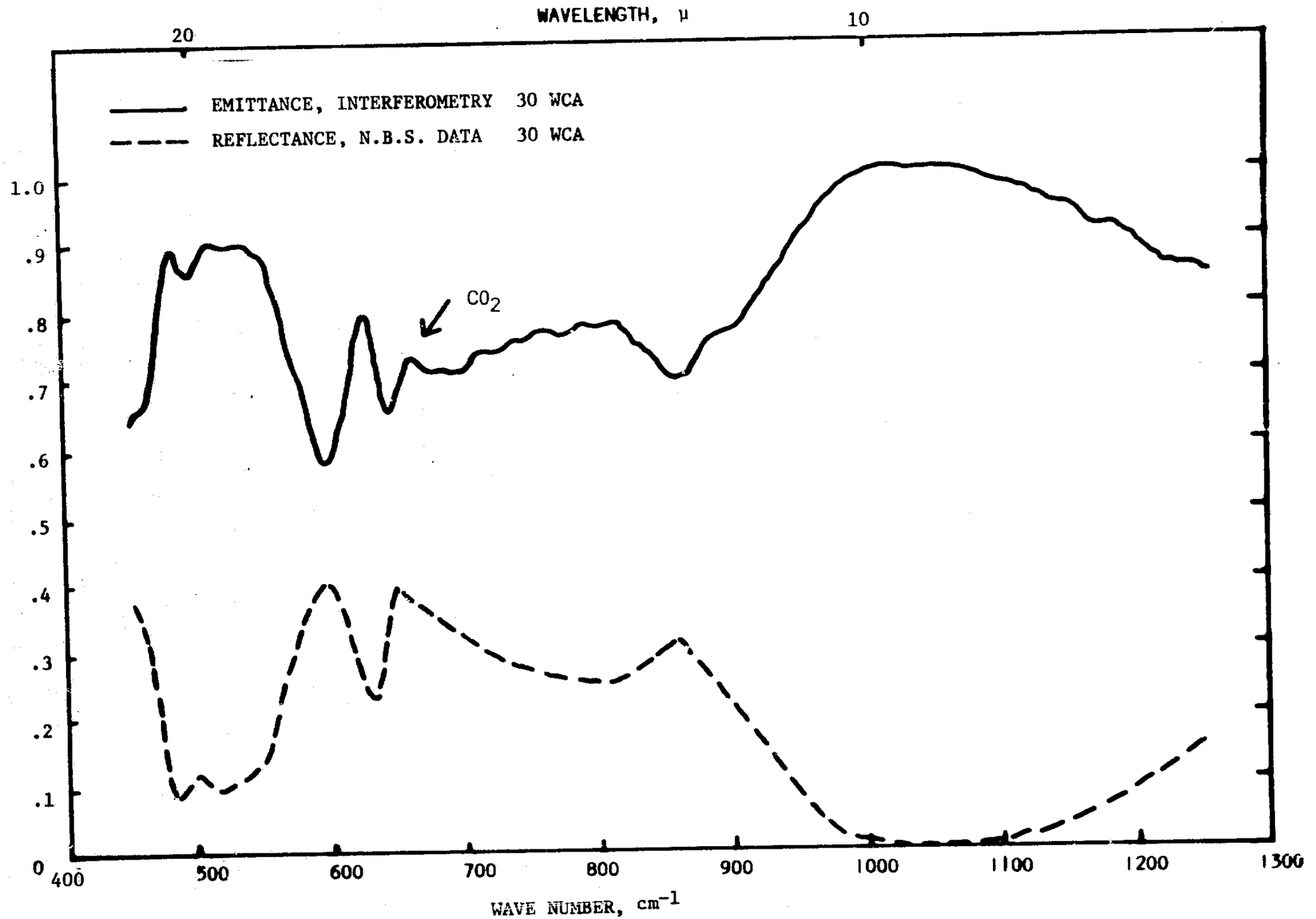

FIGURE 10. SPECTRA OF CORUNDUM POWDER

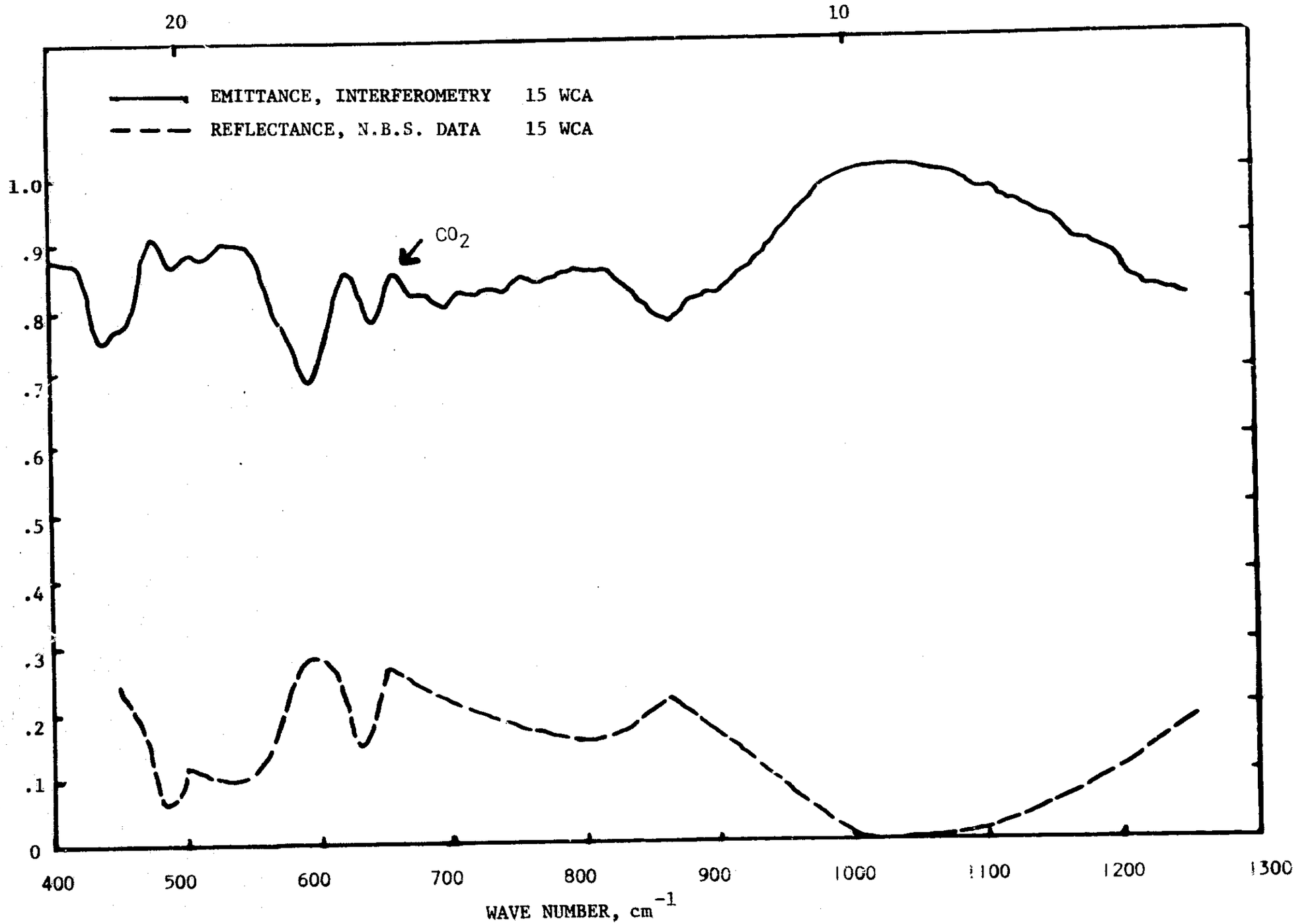

FIGURE 11. SPECTRA OF CORUNDUM POWDER

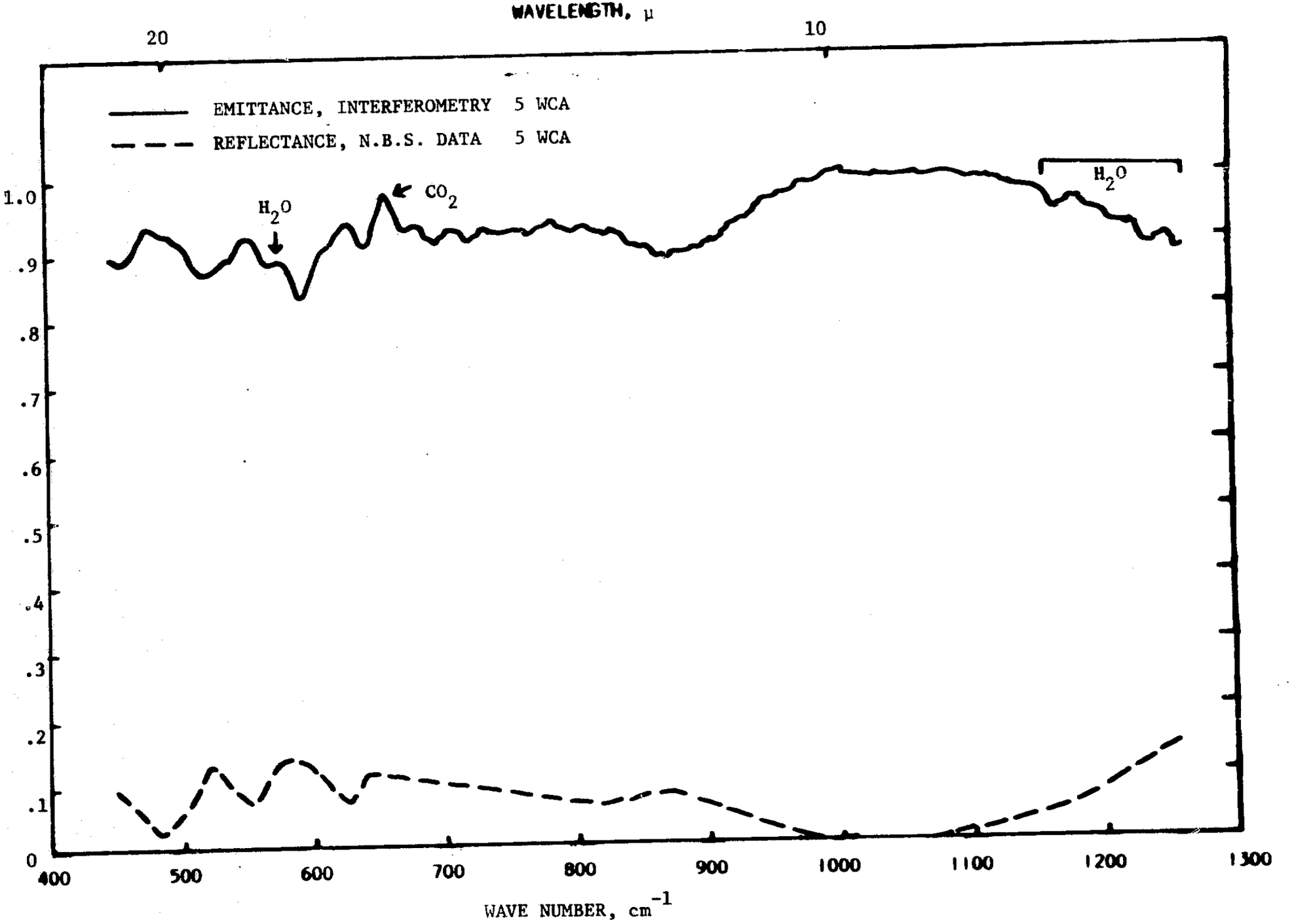

FIGURE 12. SPECTRA OF CORUNDUM POWDER

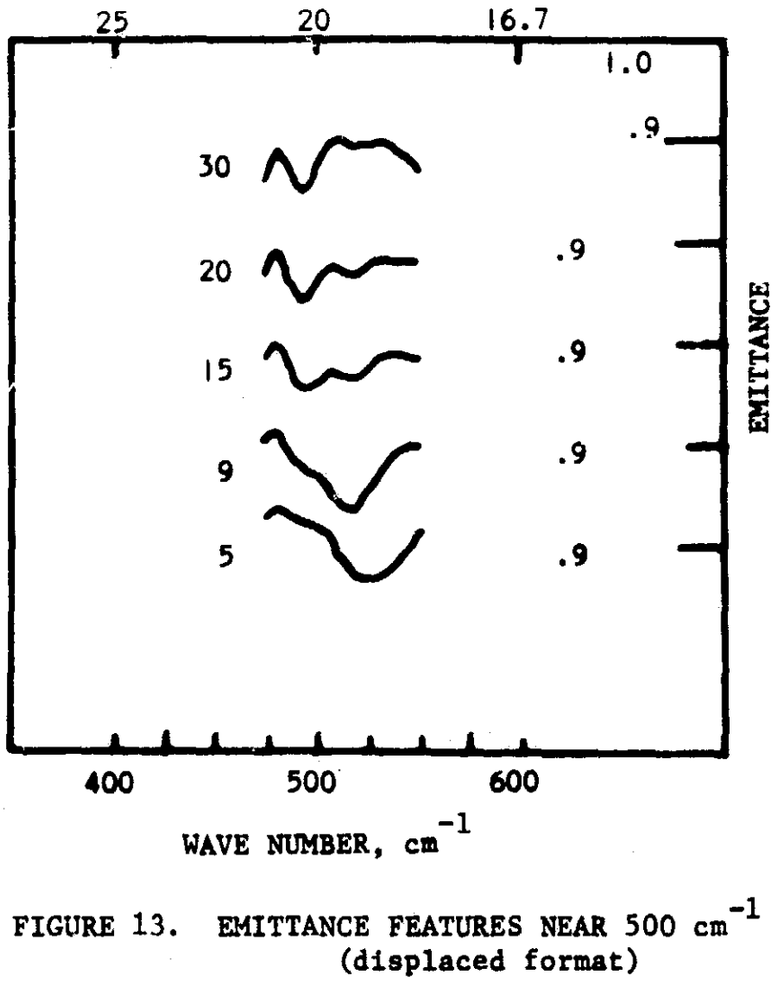

FIGURE 13. EMITTANCE FEATURES NEAR 500 cm^{-1}
(displaced format)

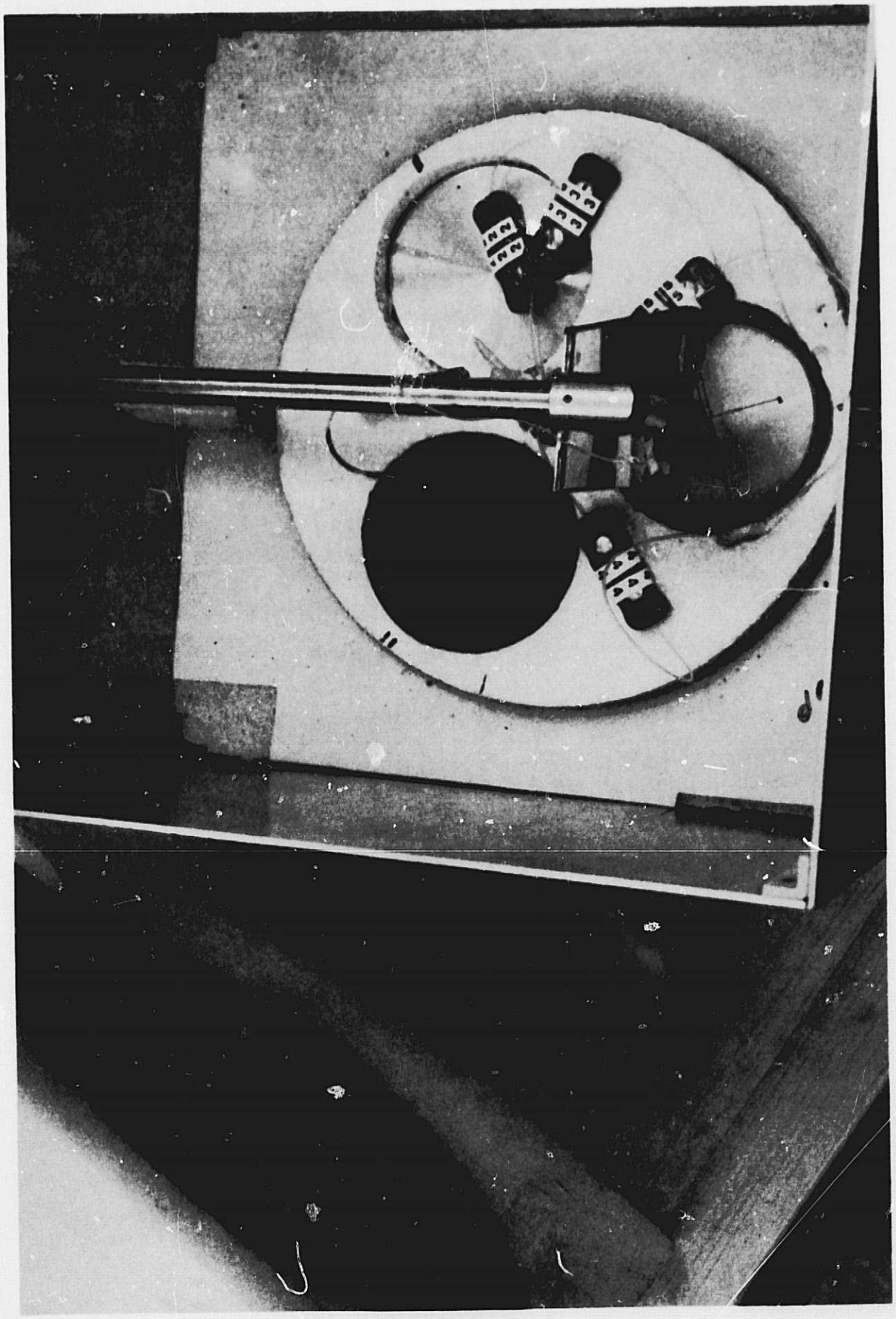

FIGURE 14. EXPERIMENTAL ENCLOSURE

intended to provide a low enough radiation background to prevent the sample from reflecting power as already discussed. The lazy susan can be turned from the outside into three positions, one for the sample, one for the reference blackbody, and one spare.

The reference blackbody is made of a round disk of 5/8" thick aluminum. Its front face is covered with concentric grooves of 30° vertex angle, coated with 3M black-velvet paint. From available data on this paint, from the calculated geometric effects of the 30° grooves, and from confirming reflectance measurements we conclude that the reference blackbody's emittance is greater than 0.99. Since the blackbody radiates only about 2 watts at maximum operating temperature into a cold shield, and is heated approximately uniformly from the back, and since the thermal conductivity of aluminum is of the order of 2 watt/degree cm, we can conclude that the disk will be isothermal to a small fraction of a degree. The measuring thermocouple is mounted in a deep groove on the back in the center of the disk and is therefore expected to read the correct temperature to within a small fraction of a degree.

The sample holder consists of a shallow pan. Its bottom is made of heavy aluminum and its walls are made of Micarta, an insulating material of low thermal conductivity. Thermocouples of 5-mil copper constantan are stretched across the diameter at two heights in an attempt to measure the powder temperature and gradients. The temperature of the aluminum bottom is also measured. We feel that the thermocouples in the powder will give a reasonable estimate of the gradient (when connected differentially), but their absolute temperature readings are more uncertain. The powder has very poor thermal conductivity and, while the lead wires are extremely thin and stretched through a low thermal gradient layer, we cannot expect perfect thermal equilibrium.

The cooled shield consists of an 8" diameter pot of 1/32" aluminum with a cylindrical tank for the cooling material welded to it. Its inside is coated with 3M black-velvet paint and in operation the

temperature differences between the outer rim and the center, where the coolant tank is fastened, are found to be less than 10°, in agreement with the design estimates.

The experiments coupling the sample enclosure and the Idealab interferometer (CsI beamsplitter) showed up a number of electrical and optical difficulties. The worst problem turned out to be due to an inadequately designed beamsplitter. Because CsI is a difficult material to polish to high tolerances, good fringes could not be obtained for the laser and white light channels. The beamsplitter was therefore fabricated from CaF_2 for the laser and white light channels and CsI for the main channel as stated above. This beamsplitter was intended to be aligned by using the laser channel, but the required coplanarity of the two pieces of optical material was not achieved. Special attachments were therefore provided to separately align the different channels. This proved to be successful and good interferograms can now be produced. We are currently running the spectra of some powders using a blackbody standard as discussed in the next section. The spectra are shown in the Appendix.

H. CALIBRATION PROCEDURE

In order to determine the emittance ε_s of the sample as a function of frequency we compare the signal S at each point of the spectrum, derived from the interferogram, with the signal S_{bb} from the blackbody source ($\varepsilon_{bb} = 1$) maintained at a temperature close to that of the sample. In making this calibration or normalization we must allow for the effect of the temperatures of the enclosures surrounding the sample as discussed previously and the detector.

We decided to operate the complete interferometer assembly in equilibrium with the temperature controlled laboratory and to record this temperature (as measured at the detector housing) of the interferometer. Fortunately, the pyroelectric detector does not require a

substantial bias power, as ordinary resistive bolometers do, and it will therefore be in temperature equilibrium with its housing (except, of course, for the desired effect of incoming radiation).

The drive of the interferometer, the preamplifiers for signal, white light and laser reference and the white light source dissipate very little power and are mounted within the interferometer enclosure but away from the cube containing the optical elements. The reference laser is mounted outside the enclosure proper.

The resultant isothermal operation of the interferometer and detector will suppress background from the optical components and it will simplify both experiment and analysis of the results.

We assume that the detector, the electronics, and the Fourier transform procedure for obtaining the spectrum from the interferogram are all linear. Therefore we can consider the signal per unit frequency interval at some frequency ν as though all other frequency components were absent.

Let Ω_s be the solid angle subtended at the sample by the aperture in the cold box that encloses the sample and let T_s, T_b, and T_o be the temperatures of the sample surface, the cold box, and the interferometer housing, respectively. Then the radiance of the beam of radiation that enters the interferometer is

$$N = \varepsilon_s B(T_s) + (1 - \varepsilon_s)(1 - \frac{\Omega_s}{2\pi})B(T_b) + (1 - \varepsilon_s)\frac{\Omega_s}{2\pi}B(T_o) \qquad (75)$$

where B is the blackbody function. The first term is direct radiation from the sample. The second term is radiation from the cold box reflected by the sample. The third term is radiation from the interferometer housing that is reflected by the sample.

Let Ω_d be the solid angle of the beam of radiation that converges on the detector after passing through the interferometer and associated optics. If we ignore losses in the interferometer, the radiance of this beam is also N during a modulating half-cycle in which the interferometer transmits from the sample to the detector. The power absorbed from the beam by the detector per unit frequency interval during this half cycle is therefore

$$W_1 = \varepsilon_d A_d \Omega_d N \tag{76}$$

where ε_d and A_d are the emittance and irradiated area of the detector.

During the nontransmitting half-cycle of the interferometer the detector is essentially in an enclosure at temperature T_o. Therefore the power input to the detector is

$$W_2 = \varepsilon_d A_d \Omega_d B(T_o) \tag{77}$$

The output modulated signal S from the detector is proportional to $W_1 - W_2$. Therefore

$$S \propto \varepsilon_d A_d \Omega_d \, [N - B(T_o)] \tag{78}$$

Thus

$$S = C\varepsilon_d A_d \Omega_d [\varepsilon_s B(T_s) + (1 - \varepsilon_s)(1 - \frac{\Omega_s}{2\pi})B(T_b) + (1 - \varepsilon_s)(\frac{\Omega_s}{2\pi})B(T_o) - B(T_o)] \tag{79}$$

where C is a constant of proportionality. As a check on this formula we note that S = 0 when $T_s = T_b = T_o$.

When the sample is replaced by the blackbody source ($\varepsilon_{bb} = 1$) at temperature T_{bb}, the signal becomes

$$S_{bb} = C\varepsilon_d A_d \Omega_d] B(T_{bb}) - B(T_o)] \tag{80}$$

Therefore

$$\frac{S}{S_{bb}} = \frac{\varepsilon_s B(T_s) + (1 - \varepsilon_s)(1 - \frac{\Omega_s}{2\pi}) B(T_b) + (1 - \varepsilon_s)(\frac{\Omega_s}{2\pi}) B(T_o) - B(T_o)}{B(T_{bb}) - B(T_o)} \tag{81}$$

On solving for ε_s we find:

$$\varepsilon_s = \frac{\frac{S}{S_{bb}} [B(T_{bb}) - B(T_o)] - (1 - \frac{\Omega_s}{2\pi})[B(T_b) - B(T_o)]}{B(T_s) - (1 - \frac{\Omega_s}{2\pi}) B(T_b) - \frac{\Omega_s}{2\pi} B(T_o)} \tag{82}$$

When the cold box is at the same temperature as the interferometer ($T_b = T_o$) the formula simplifies to

$$\varepsilon_s = \frac{S}{S_{bb}} \left[\frac{B(T_{bb}) - B(T_o)}{B(T_s) - B(T_o)} \right] \tag{83}$$

If, in addition, the blackbody source temperature matches that of the sample, the formula reduces to

$$\varepsilon_s = \frac{S}{S_{bb}} \tag{84}$$

V. COMPARISON OF THEORY WITH EXPERIMENT

Owing to the complex phenomena involved in the scattering of radiation by particulate media, we found it useful in this study to go through a repetitive cycle of checking the results of our computer modeling of the theory with experimental data followed by revision of the theory. This cycle is made necessary, we believe, because the data represent a complicated interaction of a number of separate effects, all of which are complicated in themselves. We refer here to the components of reflection previously discussed, i.e., R_e, R_i, and R_v for both coarse and fine particles. Up to this time we have found it difficult to separately determine these components experimentally. This means that the various simplifying assumptions necessary in the development of the theory can only be checked indirectly. These assumptions themselves are clearly necessary as the complex statistics of a mixture of particles prevents rigorous microscopic analysis.

Our computer programs produce the various intermediate theoretical results in graphical as well as numerical form. It is thus feasible to rapidly inspect the theoretical plots and to correlate spectral regions of poor fit to experimental data with the behavior of the input optical constants. Further, the plots of the separate components of reflectance enable one to see whether difficulties in the overall match arise from one particular theoretical reflectance component. Likewise, the ability to examine plots from either the coarse-particle model or the fine-particle model sheds some light on the regions of validity of each theory in terms of wavelength, particle size, and the values of the optical constants.

During the course of this work we have several times suspected that regions of poor fit between theory and experiment might be ascribed to incorrect values of the optical constants as derived from single-crystal data in the manner already discussed. However, we have repeatedly found that most discrepancies could be greatly reduced by improvements in our theory.

A. QUARTZ POWDER

The samples of quartz powder, previously referred to, had nominal particle-size ranges that would lead one to expect that they would provide a good test of our coarse-particle model. Figure 15a shows a comparison between experimental and theoretical reflectance spectra for quartz powder. The experimental data are for a sample having a nominal particle-size distribution of $63\ \mu < d < 125\ \mu$, and were obtained by the National Bureau of Standards for Dr. T. P. Rooney of Air Force Cambridge Research Laboratories.[31] The data taken extended to higher frequencies but a number of features believed not to be intrinsic to quartz showed up so we only used the portions of the curves shown in the figure. Some of these other features can be ascribed to water. While, as discussed previously, the particle-size distribution is somewhat different from the nominal one, a series of theoretical curves were obtained for different particle sizes for both the coarse- and fine-particle theoretical models. The fine-particle model curves were completely at variance with the experimental curve. The best fit from the coarse-particle model was obtained with a particle size of 100 μ. This curve is shown in Figure 15a. It is to be noted that this particle size is quite consistent with the nominal particle-size range. The theoretical curve has not been smoothed to simulate the effect of the finite and rather low resolution of the experimental data. Therefore the theoretical features appear sharper than those in the experimental spectrum. The excellent fit of the spectral shape is very promising for remote sensing applications. The fit is all the more remarkable considering that the theoretical reflectance is a nonlinear combination of the three component reflectances shown in Figure 15b. It is clear that not only are all three components important but that our general formula (Equation (1)) describing their interaction appears to be confirmed. In particular, the existence of an internal reflectance R_i is essential to the explanation of the observed spectrum.

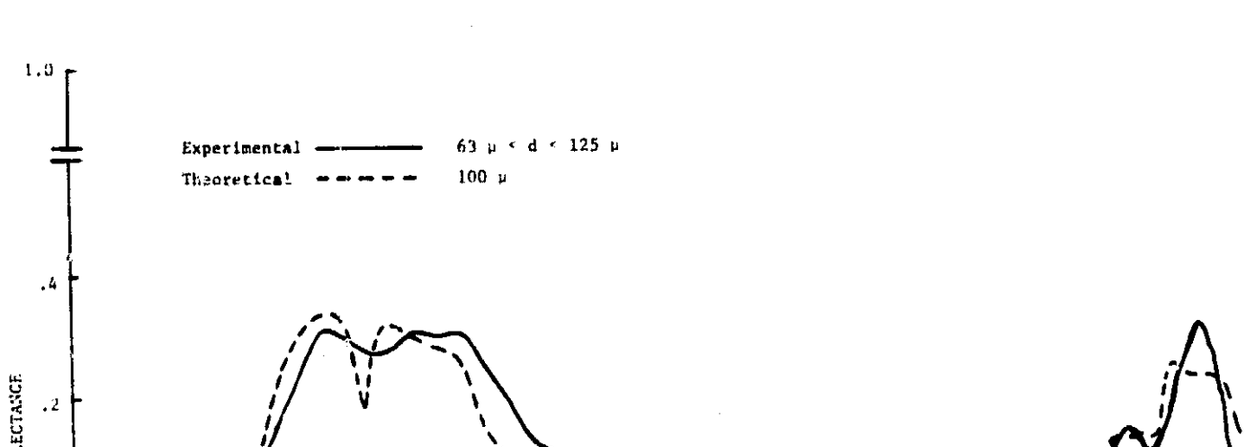

FIGURE 15a. THEORETICAL AND EXPERIMENTAL REFLECTANCE OF QUARTZ

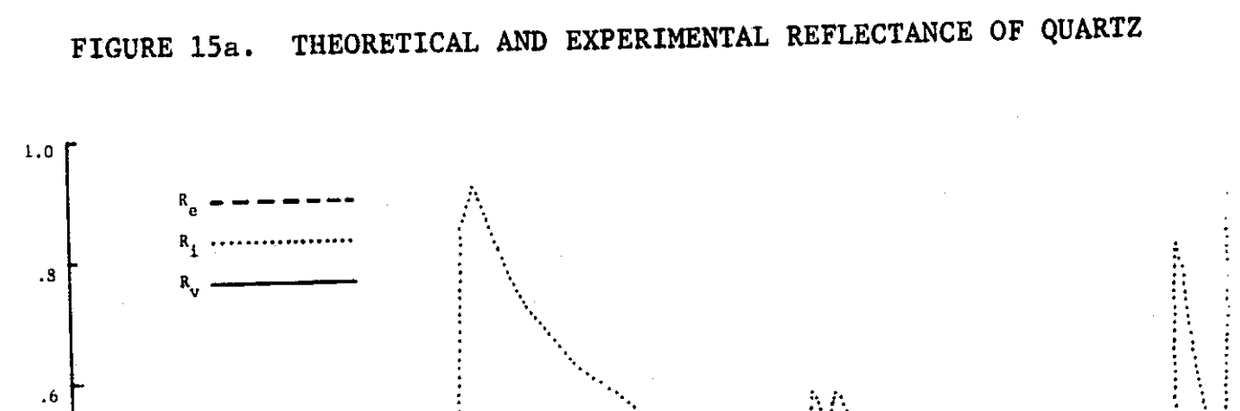

FIGURE 15b. COMPONENTS OF THEORETICAL REFLECTANCE OF QUARTZ

Figure 16 shows the same sort of comparison for particles reported to be in the range 53 μ < d < 63 μ and a theoretical curve where d is taken to be 60 μ. Once again the fit is very satisfactory. (The photograph shown in Figure 8 was taken after the fit was obtained. The "satisfactory fit" will require an explanation in terms of the actual particle-size distribution.) A comparison of Figures 15a and 16 indicates the presence of differential changes in the strengths and shapes of various features with particles size. For example, as the particle size is decreased the features around 630 cm^{-1} and 730 cm^{-1} grow in the theoretical spectrum relative to the features near 800 cm^{-1}. We observe a similar change in the experimental data. We feel that the doublet at 800 cm^{-1} represents the feature shown only as a single hump in the experimental data near 780 cm^{-1}. The resolution of the experimental data explains the smeared appearance of the band, but its slight displacement cannot be explained at the present time. However, the general trend seems to be that as the particle size is decreased, the experimental reflectance is decreased, whereas the theoretical reflectance increases. The reason appears to be that two or more opposed effects are present. The scattering coefficient S of relatively large particles increases with decreasing particle size owing to the larger number of interfaces per absorption mean free path. On the other hand, for very small particles, the efficiency of scattering decreases much more rapidly than the coarse-particle model would imply, owing to the effects of wave optics. Thus a real powder with a wide dispersion of particle sizes can show, depending on the relative volume fractions of coarser and finer particles, a trend in either direction with average particle size. Despite the relatively good agreement of the experimental and theoretical curves, these arguments suggest that we require some combination of the coarse- and fine-particle models based on the real particle-size distribution. The scanning electron micrographs do show the presence of numerous fine particles well below the nominal size range. We intend to replace the single-particles size currently used in the theoretical modeling by a simulated distribution of particle sizes in the future. Figure 17 shows some of our previously obtained data[1] for fine-quartz powder. Unfortunately,

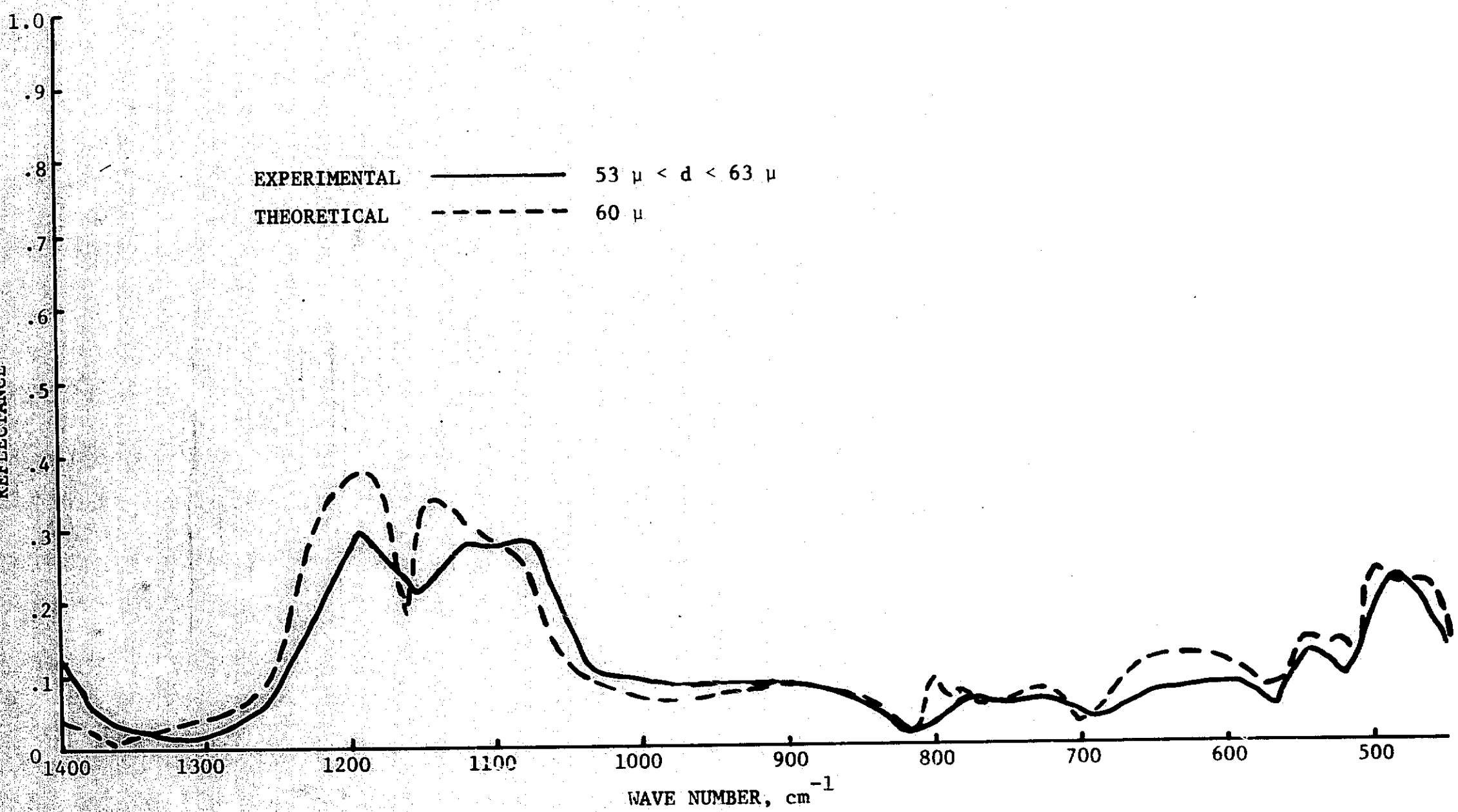

FIGURE 16. THEORETICAL AND EXPERIMENTAL REFLECTANCE OF QUARTZ POWDER

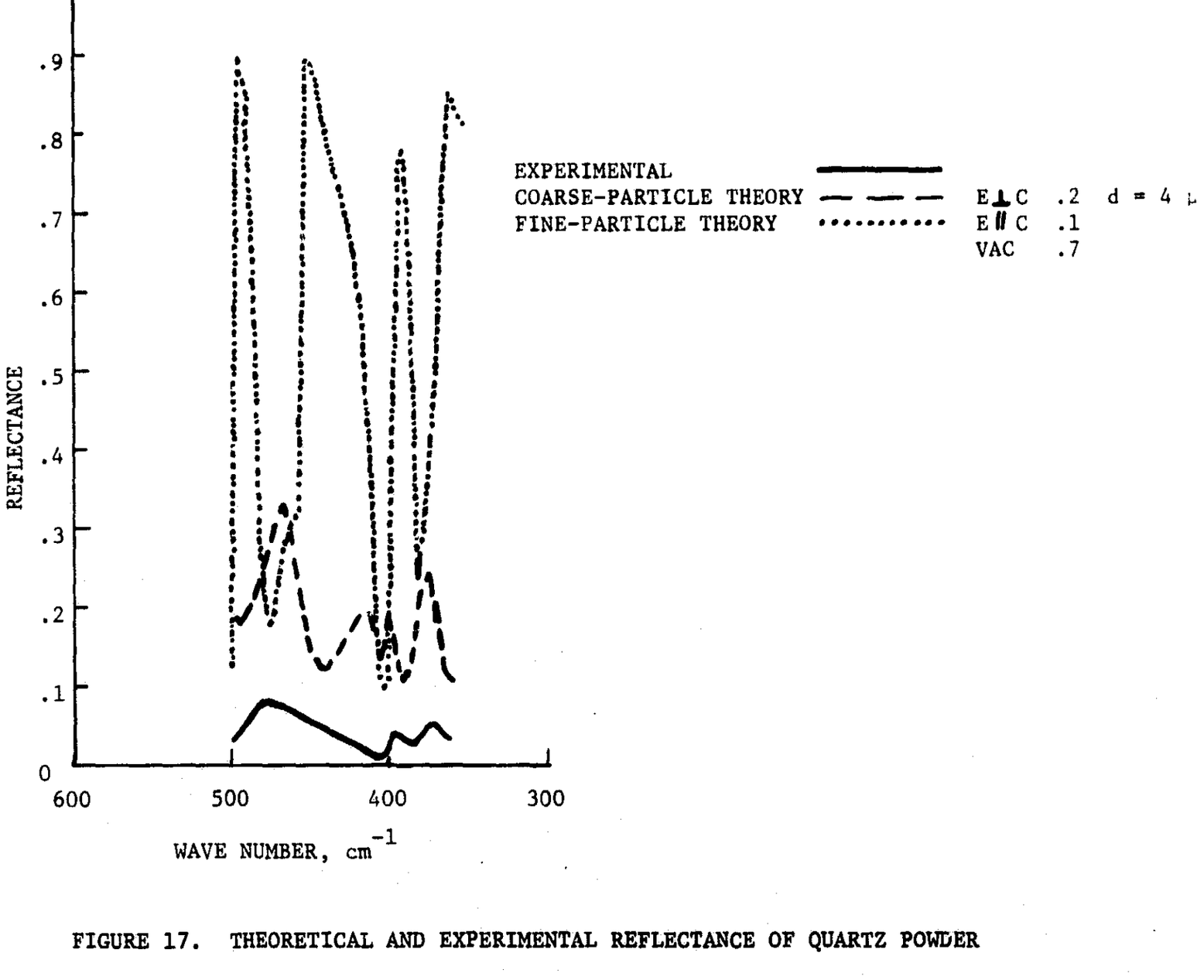

FIGURE 17. THEORETICAL AND EXPERIMENTAL REFLECTANCE OF QUARTZ POWDER

this spectrum was obtained using a biangular reflectance spectrometer. The theory does not strictly correspond to such an experimental arrangement. If one assumes the approximate validity of Lambert's cosine law, however, the only discrepancy would be that the data would appear to be arbitrarily low in absolute reflectance as the scattered radiation is not properly allowed for. The spectral shape should be unaffected, however.

It appears that a reasonable fit of the theory and the experiment, apart from the scale factor just mentioned, might be obtained if one could bridge between the fine- and coarse-particle theories. In particular, the minima near 440 cm^{-1} and 490 cm^{-1} of the coarse-particle theory would aid in fitting the fine-particle theory to the shape observed experimentally. A criterion for bridging between coarse and fine models that is discussed in the next section suggests that this may be the case.

B. CORUNDUM POWDER

Figure 9 shows the experimental emittance curves of corundum powders of various particle sizes as discussed previously. It is to be noted that for frequencies less than 1000 cm^{-1} the trend of the reflectance with particle size is by and large the same as already noted for quartz, i.e., the reflectance level decreases as particle size decreases.

We believe that, as before, there are opposing tendencies. These can be illustrated schematically by the curve shown in Figure 18 for constant volume fraction of material and constant wavelength. In this figure the portion of the curve in which the particle size is small represents the Rayleigh scattering region of wave optics including the effects of interactions between particles, in which the scattering power per unit volume falls off rapidly while absorption per unit volume remains essentially constant. The large-particle region is the domain of geometrical optics in which the scattering power per unit volume falls off with

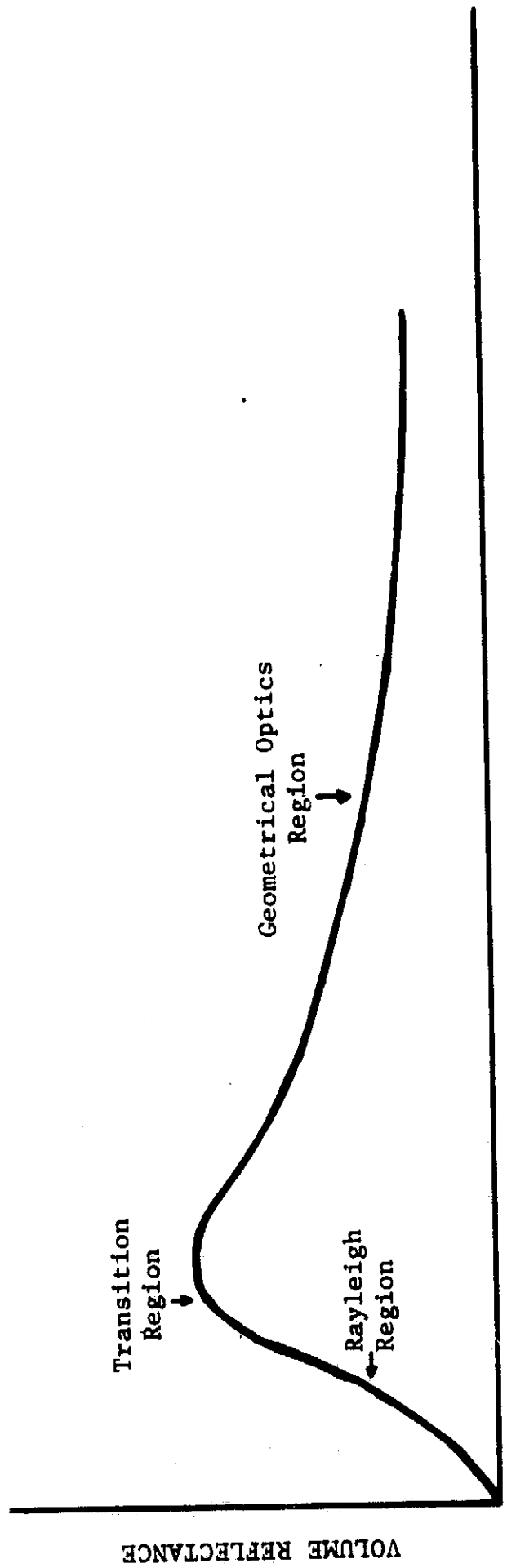

FIGURE 18. SCHEMATIC OF VOLUME REFLECTANCE VERSUS PARTICLE SIZE

increasing particle size owing to a decrease in the ratio of surface area to volume of the particles while the absorption per unit volume is again essentially constant. The intermediate region encompassing the maximum represents a bridging region where wave optics gradually merges into geometrical optics. The true volume reflectance for a mixture of particle sizes can best be imagined as an integration of this curve with a weighting factor represented by the particle-size distribution.

Now the observed decrease in reflectance with decreasing particle size (Figure 9) can be understood in terms of translation of the distribution curve towards the small-particle end of the curve if the distribution straddles the peak or is entirely in the small-particle region. On the other hand, an increase in volume reflectance with decreasing particle size would be observed if the distribution is entirely at the large-particle end. If we now refer to the high frequency portion of Figure 9 or Figure 19 (taken from NBS data[32]) we observe both trends with particle size. As the mean particle-size decreases in the series of samples (from 30 WCA down to 5 WCA) it can be seen that the reflectance in this spectral region at first increases, passes through a maximum (9, 15, and 20) and then drops rapidly (5 WCA). It should be recognized that the shape of the curve shown in Figure 18 is a function of frequency owing to variation of the optical constants. Therefore the order of the curves in Figures 9, 15, 16, and 19 is a function of frequency.

Up to this time we have utilized only a single-particle size to represent each sample rather than a particle-size distribution. We have been able to locate a maximum, such as is referred to above, for a particular case and produce the two types of variation in reflectance with particle size. However, our predicted maximum appears displaced from the observed value and the predicted rate of change in the small-particle region appears to be considerably greater than the experimental evidence warrants. This behavior is to be expected from Figure 18 for the case of a very narrow particle-size distribution.

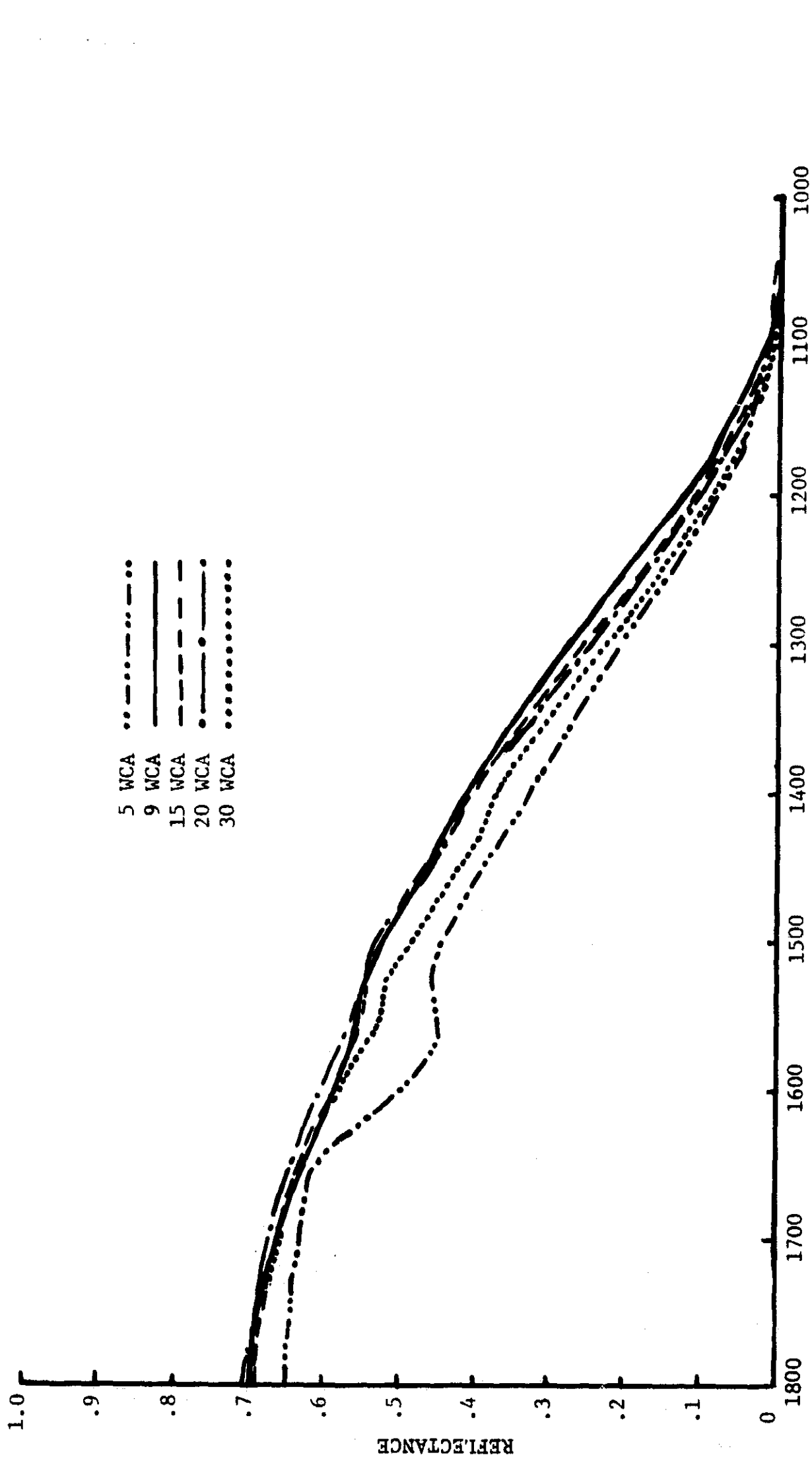

FIGURE 19. REFLECTANCE SPECTRA OF CORUNDUM POWDERS

Our main effort has been directed toward a quantitative theoretical explanation of the spectral shape of reflectance curves using principally corundum data. In Figure 20a we show experimental data for the 30 WCA sample. This curve is a composite of data that we obtained in emittance and data obtained by the National Bureau of Standards in reflectance. The reason for this composite is that water vapor bands interfered with our emission spectrum at high frequencies and that the scale used by the Bureau of Standards was difficult to transcribe with good resolution in the low frequency region where considerable structure is present. As can be seen from Figures 10-12, the two sets of data are in excellent general agreement so that we feel this composite is valid. We did remove a feature due to atmospheric carbon dioxide from our emittance data in this curve.

Figure 20a also shows a theoretical curve based on the Bragg scattering model. We found in general that the fine-particle theory fits the experimental data considerably better over most of the range than does the coarse-particle theory. However, in two regions, i.e., from 535 cm^{-1} to 595 cm^{-1} and from 400 cm^{-1} to 445 cm^{-1} we find that the coarse-particle theory provides a rather good fit where the fine-particle theory fails catastrophically. The fine- and coarse-particle regions of the theoretical curve are indicated in the legend. We have sketched in the probable trend of the curve by dotted lines in the transition regions between the regions described by the two theories. In several regions it is difficult to choose between the two theories. In particular, in the region between 730 cm^{-1} and 870 cm^{-1} both theories give a poor fit and are shown on the figure. In a few other places both theories give an acceptable fit and we have chosen to show these as parts of the fine-particle region.

It so happens that the regions where the coarse model is required are regions where the basic assumptions underlying the fine-particle theory are clearly violated. A criterion for validity of the fine-particle theory is that the backscattering coefficient S should not exceed a

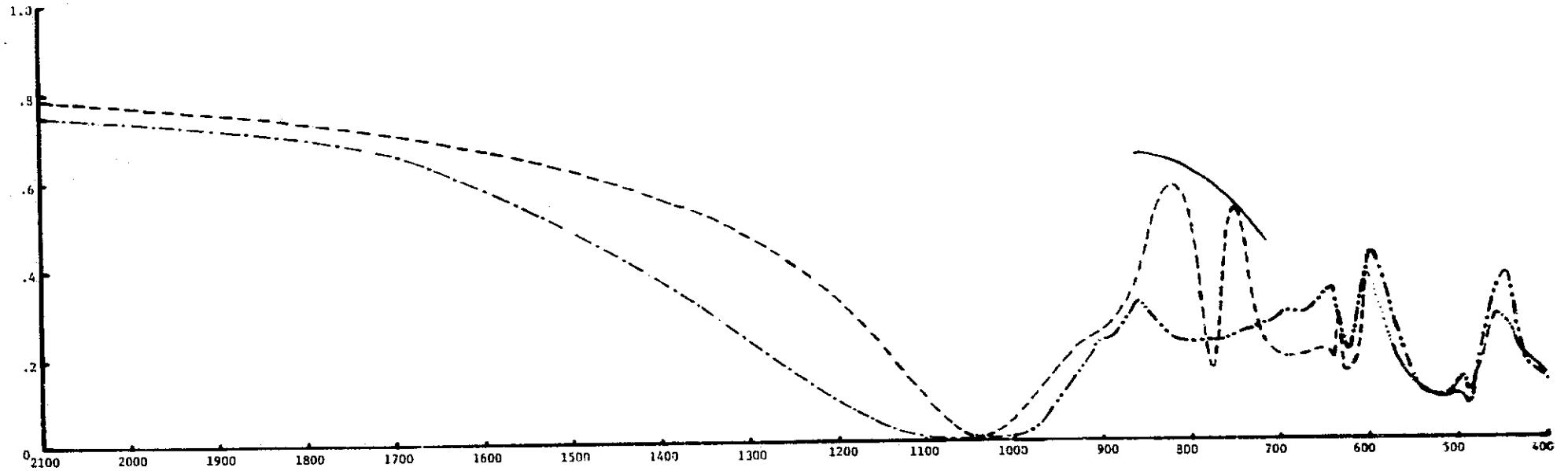

FIGURE 20a. THEORETICAL AND EXPERIMENTAL REFLECTANCE OF CORUNDUM

LEGEND:

FIGURE 20a

EXPERIMENTAL 30 WCA

REFLECTANCE (NBS) —·—·—·—

1-EMITTANCE (ADL) ··—··—··—

THEORETICAL

COARSE-PARTICLE THEORY ————

E⊥C 0.25 d = 6 μ
E∥C 0.05 d = 30 μ
VAC 0.70

FINE-PARTICLE THEORY – – – – –

E⊥C 0.2 d_e = 6 μ
E∥C 0.1
VAC 0.7

FIGURE 20b

R_e (COARSE) ————

R_e (FINE$_1$) —·—·—·—

R_e (FINE$_2$) —··—··—

R_v (FINE$_1$) – – – – –

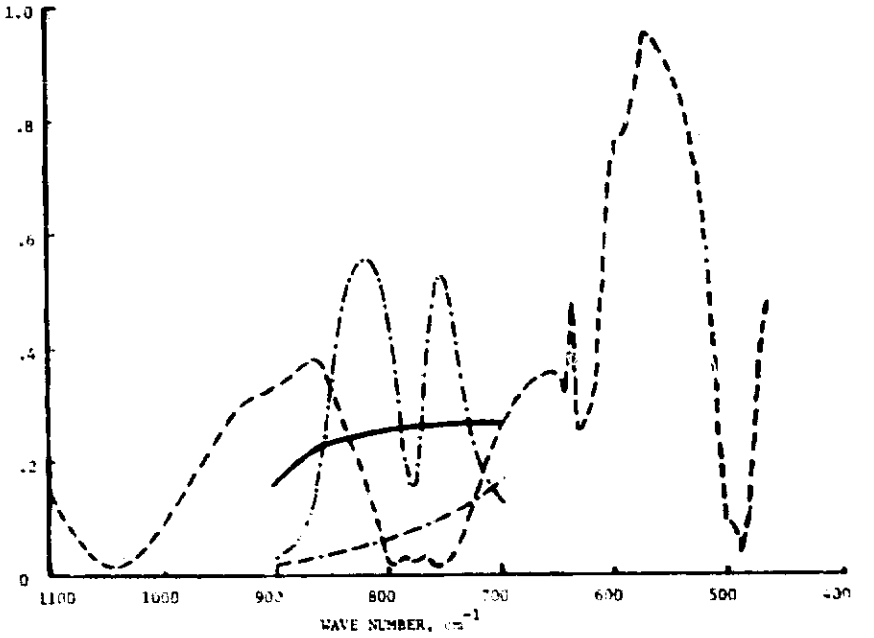

FIGURE 20b. COMPONENTS OF THEORETICAL REFLECTANCE OF CORUNDUM

backscattering coefficient S_o calculated in terms of the sum of the geometrical backscattering cross-sections for all particles in a unit of volume (Equation 63). An inspection of the computed values of S clearly indicates that the regions shown to require the coarse-particle theory have values of S greatly in excess of S_o.

The fine-particle curve shown in Figure 20a was calculated for the value of the autocorrelation length $d_e = 2\ \mu$. This length was established by examining a sequence of fits for different values of d_e. As d_e is not necessarily simply related to the average particle size, the match between the two is quite satisfactory. The proper value of d required in the coarse-particle theory is in general different from d_e since it applies to a different physical dimension. We believe that the proper coarse-particle value is essentially the average value over the distribution of particles, of thickness dimension, c, for the corundum platelets since this dimension contributes most to the interfaces per unit length of Equation 31.

The volume fraction for the overall powder was set at approximately 0.3 by porosity measurements.[5] In mixing the spectra for the two orientations of corundum we have made a simplifying assumption that the particles are randomly oriented. In the coarse-particle theory the surface contribution to scattering results in a 6:1 ratio of $E \perp C : E \parallel C$ spectra (5:1 was used in the fit shown) for the case of particles with edge ratios of 5:5:1. At the present time we have used the same weighting factors in calculating the contributions of the two spectra to the other components of our theory such as absorption and scattering by refraction. We expect to refine these factors in the future. In the fine-particle theory where a volume average is carried out, the ratio of $E \perp C : E \parallel C$ would be 2:1 for uniaxial crystallites and diffuse unpolarized radiation.

We are currently treating these weighting factors in much the same manner as we would for volume fractions of the components of a

mixture. A more refined theory for the fine-particle region, in which the Lorentz-Lorenz theory (which is based on spherical particles in spherical cavities) is modified to include ellipsoidal particles in ellipsoidal cavities, is discussed in the Appendix. This theory would allow a better treatment of anisotropic particles such as corundum and permit a clear distinction between the effects of anisotropy and the effects of separate components of a mixture. Only preliminary computer tests of this theory have been carried out to date.

We finally come to the region of poorest fit of our present theory to the experimental data, i.e., the region between 730 cm^{-1} and 870 cm^{-1}. Neither the coarse- or fine-particle theory nor a combination of these at present explains the data in this region. Our criterion is not sufficiently quantitative at present to enable us to choose the relevant theories unambiguously. We are forced therefore to examine the fundamentals of whichever theory appears to provide the best fit. The coarse-particle spectrum in this region is composed in part of a relatively large surface term R_e, shown in Figure 20b. This term is quite insensitive to particle-size effects using our present theory, and the particle-size dependence shown in Figures 9 and 19 tends to suggest that a significant modification would have to be made in R_e before a good fit could be obtained. A possible modification might be that of replacing our current assumption of a relatively smooth surface by a surface that is sufficiently rough so as to apportion the reflected radiation into a component that is reflected into the forward hemisphere as well as that reflected into the backward hemisphere. As the former component would then be included in our volume reflectance term through the factor $1-R_e$, the effect would be to reduce the surface component. However, this roughness effect would have to be quite dependent on frequency as we require a value close to the present surface term for the fit in the low frequency region of Figure 20a.

Figure 20b also shows the surface and volume components of the fine-particle theory (labeled $FINE_1$). The volume component is so small

in this region that the internal surface component, R_i, can make no difference to the observed effects (Equation 1). It should be noted that the shape of the R_v curve is very like the observed spectrum between 350 cm^{-1} and 1050 cm^{-1} and between 600 cm^{-1} and 700 cm^{-1} except for the spike at 635 cm^{-1}. The low resolution in the experiment would suppress this spike. Also shown is a modified fine-particle surface term (labeled $FINE_2$) in which only the real part of the complex refractive index of the particles was used in the Lorentz-Lorenz averaging formula (Equation 10). This treatment corresponds to the original Lorentz-Lorenz calculation for electrostatic fields in which there is no absorption in a dielectric. For the purposes of this calculation k was linearly averaged. The fit obtained was less promising than the one we have been discussing as the volume term was adversely affected. However, the two fine-particle surface terms shown in the figure indicate clearly that the fine-particle model is very sensitive to the value of k used in the Lorentz-Lorenz averaging process. On comparing Figure 20b with Figure 20a it can be seen that the experimental curve in this region lies between the two fine-particle surface term curves. This suggests that an intermediate value of k would produce a better fit. Actually, a lower effective value of k is reasonable if one takes into account the skin depth of penetration of alternating fields into a lossy dielectric. The reason is that the Lorentz-Lorenz volume averaging process would then no longer involve the central portions of particles that in fact cannot be penetrated by the field. This effect appears to be most critical when $n \ll 1$ and k has a relatively large value. The fine-particle model results shown in Figure 20a represents our current belief as to the proper method of computation for the fine-particle theory using a single-particle size. However, this theory has evolved during the course of this work and the fits shown by some of the earlier models were actually somewhat better in particular regions of the spectrum. As these models involved a previous approximation and the neglect of one factor, we would discard them were it not for the informative trend of the fits. Figure 21 shows fits for the fine-particle model during development to its present state. The theoretical curve A utilized a quadratic approximation to Equation (55).

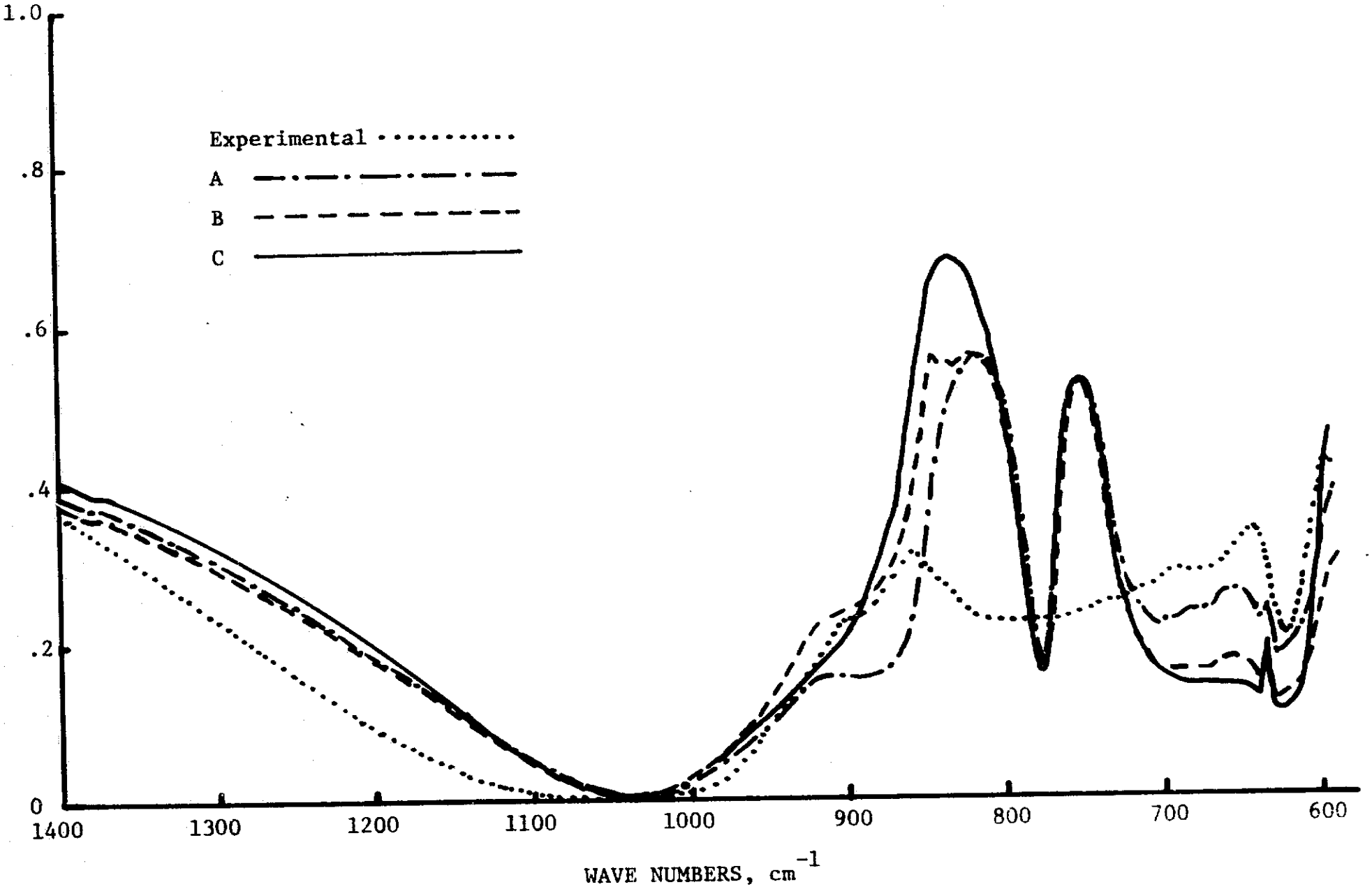

FIGURE 21. EVOLUTION OF FINE-PARTICLE THEORY

It is

$$S = \frac{\sqrt{3\pi}\,\langle \Delta n^2 \rangle}{n^2 d_e}\, G(x) \qquad (85)$$

but the factor n^2 was inadvertently neglected. This remarkable fit was improved in the 900 cm^{-1} region but made poorer in the 600-700 cm^{-1} region when the n^2 was included as shown by curve B. When the quadratic approximation was replaced by Equation (55), the results were changed to those shown by curve C. This curve is one of a family for different values of d_e and a smaller value was used in Figure 20a owing to the shape of the R_v component near 900 cm^{-1} and the somewhat improved fit between 600 cm^{-1} and 700 cm^{-1}. Unfortunately, the smaller value of d_e led to a poorer fit in the region of the minimum near 1000 cm^{-1}. We are presently uncertain as to the significance of the various poorer fits of the "better" theory. It may possibly be related to small errors in the values of the refractive index which are magnified by the exponent, or be related to the effects of particle-size distribution.

In addition to the above computations with the Bragg scattering model, we also carried out some computer modeling with the immersed-particle scattering model. The results did not fit the experimental data nearly so well as the Bragg scattering model. In spite of this we believe that the immersed-particle model deserves further attention since it is a natural extension of the Lorentz-Lorenz theory. This theory lends itself to the treatment of scattering by ellipsoidal particles which may be a considerably better approximation to the platelet geometry of corundum than is the spherical approximation already tested for this theory.

VI. CONCLUSIONS

A. SUMMARY

The research program described in this report has resulted in the development of a theory of the reflectance of mixtures of particulate materials. The general theory is somewhat differently constructed for use in two distinct regimes. The methods of geometrical optics are used to compute the components of the theory when the particle size is coarse compared to the radiation wavelength, while an approach based on Bragg scattering and the Lorentz-Lorenz theory of dielectrics is used for fine-particulate materials. Separate comparisons of these theories and experimental data for coarse quartz powder and fine corundum powder indicate that the infrared spectral shapes of the materials can be predicted for the most part using the appropriate regimes of the theory. In addition, the theory predicts qualitatively many of the particle-size dependent changes in the spectra. Toward the end of this work, a criterion for a decision as to the regime of applicability of each of the two theories was discovered and it was found to fit the experimental data qualitatively. This criterion involves the optical constants of the materials in such a way as to explain to some degree why it is possible to find adjoining spectral regions where either of the two subtheories may be applicable. The region in which neither theory is applicable is expected to involve some sort of compromise between the two extreme theories and we hope to be able to empirically fit this region when the criterion for selection is refined.

The theory has been programmed for rapid computation using high speed digital computers. The intermediate components and plotting programs allow rapid useful comparison of the data with experimental results. The physical nature of the theory is such as to allow easy access to the effects of different geometries and particle statistics unlike the Mie theory.

A Michelson interferometer has been used to gather emission data for a limited number of materials. We plan to extend the use of this powerful tool in any future work. We have also relied on data obtained from other sources in fitting the theory to experimental observations. We believe that the development of this theory will greatly extend the usefulness of the present capability to gather remote compositional information by infrared spectroscopy.

B. SUGGESTIONS FOR FURTHER WORK

During the course of this work we have continually tried to refine our theoretical treatment. As the subject matter is inherently complex, many approximations have been required. We have continually attempted to refine and improve the theory but inevitably we have been unable to explore a number of alternative approaches that seemed to give high promise. In addition, the late arrival of our new interferometer and experimental difficulties encountered in using it have delayed many of the critical experiments we intended to carry out.

The topics for future investigation that occur to us at this time are:

1. The Effect of Skin Depth on the Lorentz-Lorenz Theory--We presently believe that the only spectral region of poor fit of our theory to experimental data may be explained by the use of an improper value of k in the Lorentz-Lorenz averaging process. We intend to conduct further computer simulation experiments in this regard.

2. Criterion for Decision as to the Proper Subtheory to be used as a function of the optical constants and radiation wavelength as well as particle size. The criterion just discovered should be refined so that a quantitative choice can be made as well as an attempt to smoothly bridge between the two subtheories. We expect to be guided in this by the experimental data such as we have been using. To this end we propose to make

measurements on coarse corundum and fine quartz to supplement our present information on fine corundum and coarse quartz.

3. Evaluation of the Effect of Surface Roughness--The scanning electron micrographs currently in our possession have recently been contoured. We plan to extract from these contours sufficient detailed statistical information so as to be able to properly evaluate the degree to which the surface term has been misrepresented by our assumption of a gentle undulating surface. Our new scanning electron microscope facility should enable further use to be made of this powerful technique for surface evaluation. To this end it would be very helpful if we could find an experimental technique for distinguishing the components of our theory, R_e, R_i, and R_v. One experiment we have discussed for this purpose is the measurement of the infrared emission spectrum of a roughened sapphire crystal. The scanning electron microscope would be invaluable here as a technique for accurately assessing the degree of surface roughness of the sample.

4. The Effects of Particle Agglomeration--We believe our current theory can be modified to combine the coarse- and fine-particle theories in such a way as to allow for the effects of particle agglomeration. Once again the scanning electron microscope will be helpful as a method of identifying the degree of agglomeration for our particular samples. We need to understand the degree of importance of both surface roughness and particle agglomeration in order to assess the effects of these two variables on the spectra of unknowns.

5. Experimental Studies of Mixtures--Our experimental work to date has largely involved the use of the spectra of different orientations of a single material in order to simulate mixtures. We plan to remedy this by making experimental measurements on mixtures of quartz and corundum as well as garnet and glass. The optical constants of the latter two materials must be obtained so as to be able to usefully examine the spectra of powders of these materials. A recent paper in the literature[34]

has suggested a simple computer technique of extracting the optical constants from either reflectance or transmittance measurements on homogeneous isotropic materials. The study of isotropic materials would simplify some of the assumptions we have required for dealing with anisotropic materials. A modification of our present Lorentz-Lorenz theory to ellipsoidal particles has already begun. This modification permits the proper distinction to be made between the effects of anisotropy of one material and the effects of distinct materials. We plan to further develop this approach and use it in conjuction with the immersed particle model.

6. The Effects of Real Particle-Size Distributions--An easily remedied defect of our current theories is the use of single-particle sizes to represent real distributions. As discussed in Section V, we believe this improvement should go a long way toward improving the quantitative nature of our fits between theory and experiment.

7. Other Improvements--We intend to reprogram our theory in such a way as to permit simulation of the scanning function of real spectrometer so that the comparisons between theory and experiment will no longer suffer from differing resolutions between them. We also plan to restructure the coarse-particle model so as to utilize the 6-beam approach already used in the fine-particle theory.

8. The Unscrambling of Real Unknowns--A strategy for computer unscrambling of the spectra of unknowns will be required for use in any remote sensing mission. We believe that a start should be made on this topic.

Obviously, we cannot carry out all of these tasks with the same priority. We would plan to give our first attention to Tasks 1, 2, 5, and 6.

VII. APPENDIX

A. OVERALL REFLECTANCE FORMULA

The scattering of radiation from the collimated beam acts as a source term for the diffuse radiation in the powder. When this source term is added to the Kubelka-Munk differential equations, we obtain

$$\frac{dI}{dx} = -(K + S)I + SJ + \frac{1}{2} SI_c \qquad (A1)$$

$$-\frac{dJ}{dx} = -(K + S)J + SI + \frac{1}{2} SI_c \qquad (A2)$$

In these equations I and J are the diffuse radiation flux densities in the positive and negative x-directions, respectively, while I_c is the flux density of the collimated beam, given by Equation (65). The term $SI_c/2$ is the scattering per unit volume of the collimated beam.

Equations (A1) and (A2) have solutions of the form

$$I = Ce^{-\gamma x} + a(1 - R_e)I_o e^{-\beta x} \qquad (A3)$$

$$J = R_v Ce^{-\gamma x} + b(1 - R_e)I_o e^{-\beta x} \qquad (A4)$$

where C is an arbitrary constant and

$$\gamma = (K^2 + 2KS)^{1/2} \qquad (A5)$$

$$\beta = S + K/2 \qquad (A6)$$

$$R_v = (K + S - \gamma)/S \qquad (A7)$$

$$a = S(K + 2S + \beta)/2(\gamma^2 - \beta^2) \qquad (A8)$$

$$b = S(K + 2S - \beta)/2(\gamma^2 - \beta^2) \qquad (A9)$$

Equations (A3) and (A4) already include the boundary condition for large x that $J/I \to R_v$.

The constant C is determined by the boundary condition at the surface of the powder (x = o), which is

$$I(o) = R_i J(o) \tag{A10}$$

On substituting for I(o) and J(o) from (A3) and (A4) into (A10), and then solving for C we find that

$$C = \frac{(1 - R_e)(bR_i - a)I_o}{(1 - R_i R_v)} \tag{A11}$$

The total radiation J_o reflected from the surface of the powder is the sum of the specular and diffuse components:

$$J_o = R_e I_o + (1 - R_i)J(o) \tag{A12}$$

On substituting for J(o) from (A4) and taking the ratio of J_o to I_o we find for the overall reflectance:

$$R = R_e + \frac{(1 - R_e)(1 - R_i)S[(K + 2S - \beta) - R_v(K + 2S + \beta)]}{2(\gamma^2 - \beta^2)(1 - R_v R_i)} \tag{A13}$$

With the help of (A5,6,7), (A13) reduces to the form given in Equation (1).

B. FRACTION f_b OF RADIATION BACKSCATTERED BY REFRACTION

In Figure A1 a ray incident on a random interface is represented by the point P on the surface of a sphere of unit radius. The cone of half-angle ϕ_m that contains the refracted rays produced by all orientations of the interface is represented by the small-circle AEBD on the sphere. The plane of the great-circle ACB is parallel to the surface of the powder.

On the assumption that the refracted radiation is uniformly distributed over the cone, we can write for the fraction f_b of the radiation that is backscattered:

$$f_b = \frac{\text{Area ACBD}}{\text{Area AEBD}} \tag{A14}$$

The area of the spherical cap is

$$\text{AEBD} = 2\pi(1 - \cos\phi_m) \tag{A15}$$

The area ACBD can be expressed as

$$\begin{aligned}\text{ACBD} &= \text{APBD} - \text{APBC} \\ &= 2\delta(1 - \cos\phi_m) - \text{APBC}\end{aligned} \tag{A16}$$

where δ is the angle APC.

Now APBC is a spherical triangle since its sides are all arcs of great circles. Therefore, since the area of a spherical triangle on a unit sphere is the sum of the three angles less π,

$$\text{APBC} = 2\varepsilon + 2\delta - \pi \tag{A17}$$

where ε is the angle PAC.

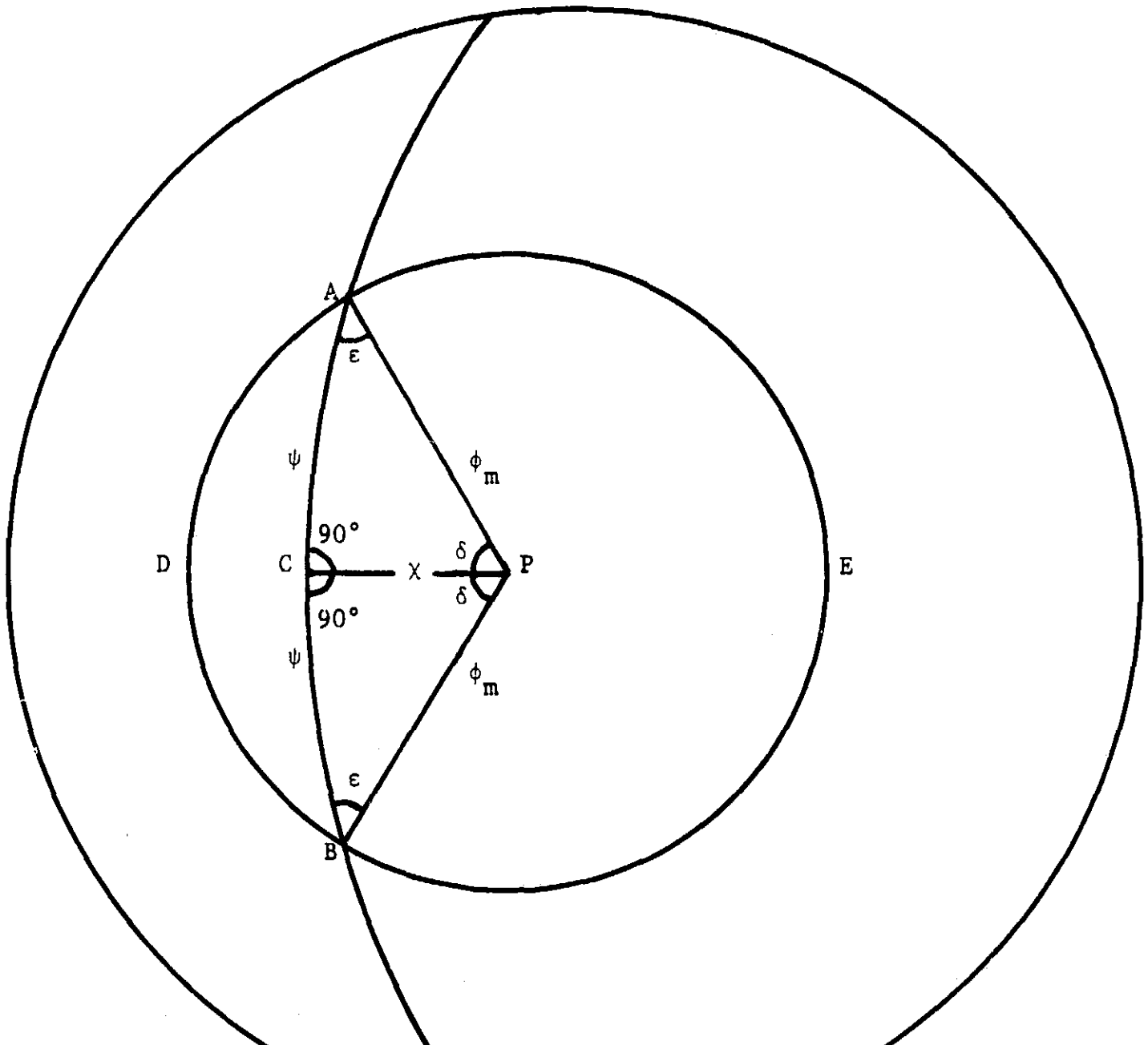

FIGURE A1. DIAGRAM FOR CALCULATING THE BACKSCATTERING DUE TO REFRACTION

Also from spherical trigonometry,

$$\sin\varepsilon = \frac{\sin\chi}{\sin\phi_m} \tag{A18}$$

and

$$\cos\delta = \frac{\tan\chi}{\tan\phi_m} \tag{A19}$$

where χ is the arc CP.

With the help of Equations (A15-A19), Equation (14) takes the form shown in Equation (21).

C. GENERALIZATION OF THE LORENTZ-LORENZ THEORY TO ELLIPSOIDAL PARTICLES

The original Lorentz-Lorenz theory expresses the dielectric constant of a material in terms of the electric polarizibility of the molecules (assumed to be spherical) of the material. We have extended the theory to the case of spherical particles of macroscopic size. Here we extend the theory still further to the case of randomly oriented ellipsoidal particles. Such particles, with a suitable choice of the axes of the ellipsoids, will approximate platelet and needle-shaped particles as well as rounded particles.

As in the Lorentz-Lorenz theory we consider that the field acting on a given particle is the field that would exist in a cavity of the same shape as the particle if the particle were removed, but with the dipole moments of all other particles frozen in magnitude and direction. Let E_x, E_y, E_z be the electric field components in the medium referred to axes aligned with the principal axes of the ellipsoid. Then the field components E_x^c, E_y^c, E_z^c in the cavity are

$$E_x^c = E_x(1 + L\chi) \tag{A20}$$

$$E_y^c = E_y(1 + M\chi) \tag{A21}$$

$$E_z^c = E_z(1 + M\chi) \tag{A22}$$

where χ is the effective electric susceptibility of the medium and L, M, and N are depolarization factors that depend on the shape of the ellipsoid.[35] For the spherical case, $L = M = N = 4\pi/3$. For the case of a disk-shaped ellipsoid with short axis in the x-direction $L = 4\pi$, $M = N = 0$.

From electrostatic theory the polarization produced in the particle by the field in the cavity has components

$$P_x^p = \frac{\chi_p}{1 + L\chi_p} E_x^c \tag{A23}$$

$$P_y^p = \frac{\chi_p}{1 + M\chi_p} E_y^c \tag{A24}$$

$$P_z^p = \frac{\chi_p}{1 + N\chi_p} E_z^c \tag{A25}$$

where χ_p is the electric susceptibility of the particle.

On substituting for E_x^c, E_y^c, E_z^c from (A20-22) we get

$$P_x^p = \frac{\chi_p(1 + L\chi)}{(1 + L\chi_p)} E_x \tag{A26}$$

$$P_y^p = \frac{\chi_p(1 + M\chi)}{(1 + M\chi_p)} E_y \tag{A27}$$

$$P_z^p = \frac{\chi_p(1 + N\chi)}{(1 + N\chi_p)} E_z \tag{A28}$$

Let θ be the angle that the x-axis of the ellipsoid makes with the total field $\vec{E}$ in the medium. Then

$$E_x = E \cos\theta \tag{A29}$$

and

$$P_x^p = \frac{\chi_p(1 + L\chi)}{(1 + L\chi_p)} E \cos\theta \tag{A30}$$

The average component of P_x^p in the direction of $\vec{E}$ is found by multiplying P_x^p by $\cos\theta$ and averaging over all values of θ. The result is

$$\overline{(P_x^p)_{\vec{E}}} = \frac{1}{3} \frac{\chi_p(1 + L\chi)}{(1 + L\chi_p)} E \tag{A31}$$

On adding the similar contributions from P_y^p, P_z^p we find for the average electric dipole moment of the particle

$$M = \frac{1}{3} EV \left[\frac{\chi_p(1 + L\chi)}{(1 + L\chi_p)} + \frac{\chi_p(1 + M\chi)}{(1 + M\chi_p)} + \frac{\chi_p(1 + N\chi)}{(1 + N\chi_p)} \right] \tag{A32}$$

where V is the volume of a particle.

We next express M in terms of the susceptibility of the medium:

$$\chi = \frac{fME}{V} \tag{A33}$$

where f is the volume fraction of the particles.

On substituting for M from (A32) into (A33) and solving for χ we obtain the result

$$\chi = \frac{f\left[\frac{\chi_p}{1 + L\chi_p} + \frac{\chi_p}{1 + M\chi_p} + \frac{\chi_p}{1 + N\chi_p}\right]}{3 - f\left[\frac{L\chi_p}{1 + L\chi_p} + \frac{M\chi_p}{1 + M\chi_p} + \frac{N\chi_p}{1 + N\chi_p}\right]} \qquad \text{(A34)}$$

This formula reduces to the usual Lorentz-Lorenz result for the case of spherical particles where $L = M = N = 4\pi/3$.

In the case of a mixture of particles (A34) becomes

$$\chi = \frac{\sum_j f_j\left[\frac{\chi_j}{1 + L_j\chi_j} + \frac{\chi_j}{1 + M_j\chi_j} + \frac{\chi_j}{1 + N_j\chi_j}\right]}{3 - \sum_j\left[\frac{L_j\chi_j}{1 + L_j\chi_j} + \frac{M_j\chi_j}{1 + M_j\chi_j} + \frac{N_j\chi_j}{1 + N_j\chi_j}\right]} \qquad \text{(A35)}$$

where χ_j is the electric susceptibility of mineral j.

We can generalize the result still further by letting the particles be birefringent, in which case different values of χ_j, e.g., χ_{L_j}, χ_{M_j}, χ_{N_j}, must be associated with the three ellipsoid axes. The formula then becomes

$$\chi = \frac{\sum_j f_j\left[\frac{\chi_{L_j}}{1 + L_j\chi_{L_j}} + \frac{\chi_{M_j}}{1 + M_j\chi_{M_j}} + \frac{\chi_{N_j}}{1 + N_j\chi_{N_j}}\right]}{3 - \sum f_j\left[\frac{L_j\chi_{L_j}}{1 + L_j\chi_{L_j}} + \frac{M_j\chi_{M_j}}{1 + M_j\chi_{M_j}} + \frac{N_j\chi_{N_j}}{1 + N_j\chi_{N_j}}\right]} \qquad \text{(A36)}$$

The χ's are related to the optical constants as follows:

$$\chi = \frac{\varepsilon - 1}{4\pi} = \frac{(n - ik)^2 - 1}{4\pi} \tag{A37}$$

$$\chi_{L_j} = \frac{(n_{L_j} - ik_{L_j})^2 - 1}{4\pi}, \text{ etc.} \tag{A38}$$

The factors L, M, N are related to the semi-axes a, b, c of the ellipsoid as follows:[35]

$$L = -4\pi abc \frac{\partial \phi}{\partial a^2} \tag{A39}$$

$$M = -4\pi abc \frac{\partial \phi}{\partial b^2} \tag{A40}$$

$$N = -4\pi abc \frac{\partial \phi}{\partial c^2} \tag{A41}$$

where

$$\phi = \int_0^\infty \frac{du}{\sqrt{(a^2 + u)(b^2 + u)(c^2 + u)}} \tag{A42}$$

In the case of an oblate spheroid for which $b = c = a/\sqrt{1 - e^2}$

$$L = 4\pi\left(\frac{1}{e^2} - \frac{\sqrt{1 - e^2}}{e^3} \sin^{-1} e\right) \tag{A43}$$

$$M = N = 2\pi - L/2 \tag{A44}$$

For example, for platelets like corundum with $b = c = 5a$, $L = 9.43$ and $M = N = 1.57$.

In the case of a prolate spheroid, for which $b = c = a\sqrt{1 - e^2}$,

$$L = 4\pi\left(\frac{1}{e^2} - 1\right)\left(\frac{1}{2e}\log\frac{1+e}{1-e} - 1\right) \qquad (A45)$$

$$M = N = 2\pi - L/2 \qquad (A46)$$

D. SPECTRA OF POWDERS USING INTERFEROMETER SYSTEM

At the conclusion of this work we succeeded in using our new interferometer system in conjunction with the sample enclosure, already discussed, to obtain emittance spectra of powders. The first sample run was the corundum WCA 30 powder previously discussed. We felt it necessary to rerun this sample as a final check on our overall system. The emittance spectrum is shown in Figure A2. Thermocouples mounted at known positions in the powder permitted an extrapolation to the temperature of the surface. This temperature proved to be in error by a few degrees, and we followed the procedure discussed in our previous work[5] to obtain the true surface temperature. The results, which extend to lower frequencies, are consistent with our previous results and thereby confirm the validity of our procedures. We note the absence of the 660 cm^{-1} CO_2 feature that resulted from inadequate calibration of our previous data. The present data were taken using 10 cm^{-1} resolution and the features were clearly discernible in a single 30-second scan. The data shown represent 20 co-additions. This powder had a porosity of $f_{vac} = 0.612$.

We then ran a sample of a relatively fine-grain quartz powder. The particle-size distribution of the sample was examined by optical microscopy, using the split-image technique for measurement of particle diameter. The volume fraction distribution obtained in this way is bimodal. Particle diameters between 10 and 20 μ constitute the bulk of the material with peaks near 12 and 19 μ. The porosity was measured to be $f_{vac} = 0.761$. Once again the temperature measurement was somewhat uncertain. We chose the curve shown in Figure A2 by the same technique

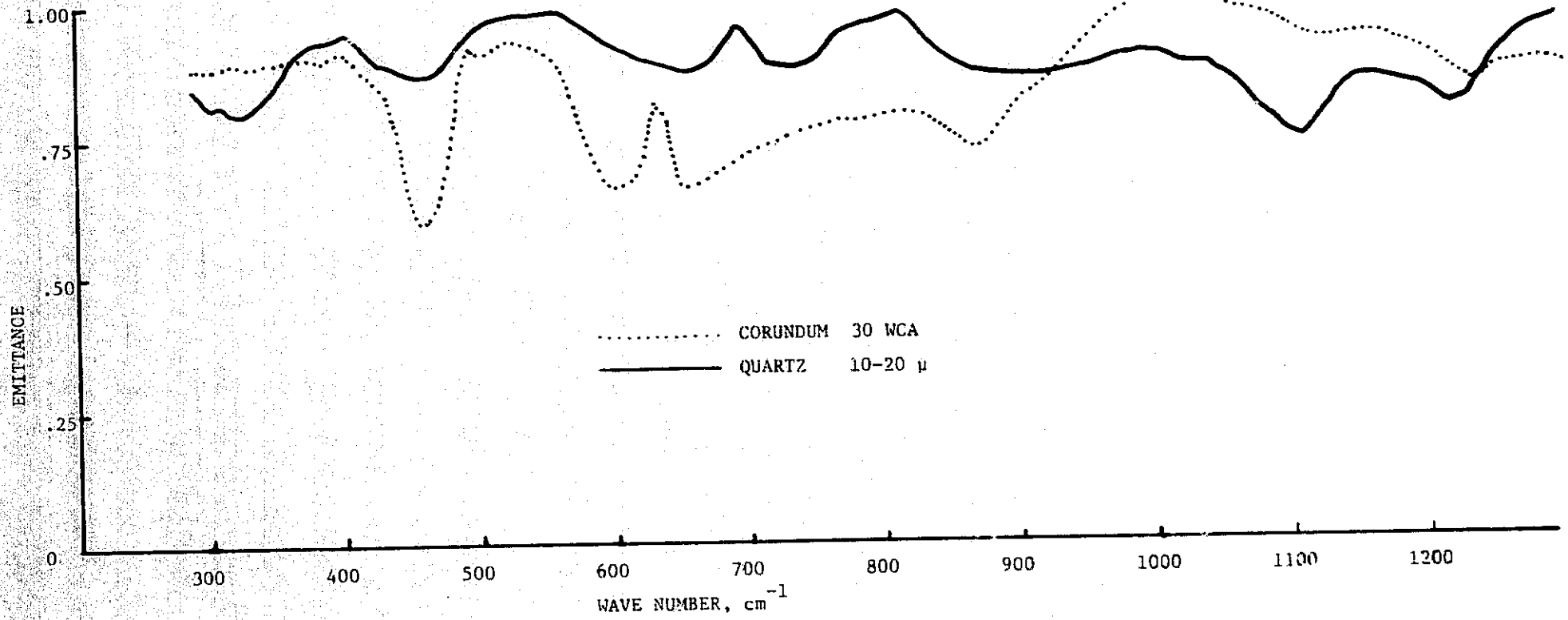

FIGURE A2. EMITTANCE SPECTRA OF MINERAL POWDERS

of assuming an emittance value of unity at a Christensen frequency as discussed in Reference 5. For completely unknown samples, it will be necessary to refine our temperature measuring technique.

VIII. REFERENCES

1. J. R. Aronson, A. G. Emslie, R. V. Allen and H. G. McLinden, J. Geophys. Res. 72, 687 (1967).

2. A. G. Emslie, in Progress in Astronautics and Aeronautics, (Academic Press, Inc., New York, 1966) Vol. 18.

3. J. R. Aronson, A. G. Emslie and H. G. McLinden, Science 152, 345 (1966).

4. J. R. Aronson and H. G. McLinden, in Progress in Astronautics and Aeronautics, (Academic Press, Inc. New York, 1966) Vol. 18.

5. J. R. Aronson, A. G. Emslie, T. P. Rooney, I. Coleman and G. Horlick, Appl. Opt. 8, 1639 (1969).

6. W. A. Hovis, Jr., and W. R. Callahan, J. Opt. Soc. Am. 56, 639 (1966).

7. R. J. P. Lyon, NASA C R 100, Washington, D.C. (1965).

8. G. R. Hunt and R. K. Vincent, J. Geophys. Res. 73, 6039 (1968).

9. E. E. Bell and I. L. Eisner, J. Opt. Soc. Am. 46, 303 (1956).

10. R. S. Vickers and R. J. P. Lyon, in Progress in Astronautics and Aeronautics, (Academic Press, Inc., New York, 1967) Vol. 20.

11. A. Schuster, Astrophys. J. 21, 1 (1905).

12. P. Kubelka and F. Munk, Zeits Tech. Physik 12 593 (1931).

13. S. Chandrasekhar, Radiative Transfer, (Clarendon Press, Oxford (1950).

14. G. Mie, Ann. Phys. 25, 377 (1908).

15. J. E. Conel, J. Geophys. Res. 74, 1614 (1969).

16. A. S. Barker, Jr., Phys. Rev. 132, 1474 (1963).

17. W. G. Spitzer and D. A. Kleinman, Phys. Rev. 121, 1324 (1961).

18. A. D. Little, Inc. proposal to National Aeronautics and Space Administration, Washington, D.C. March 15, 1966 (Mariner).

19. G. A. Vanasse and H. Sakai, in Progress in Optics, (John Wiley Inc., New York, 1967) Vol. 6.

20. J. Connes, Rev. Opt. 40, 45, 116, 171, 231 (1961), Translation NAVWEPS Report 8099 NOTSTP 3157.

21. L. Mertz, Transformations in Optics, (John Wiley, New York, 1965).

22. P. Fellgett, Thesis, University of Cambridge, 19..

23. L. W. Chaney, U. Michigan Technical Report, Contract NASr-54(03), (1967).

24. Barnes Engineering Company, Bulletin 2..20.

25. Private Communication from J. Pritchard, Idealab, Franklin, Massachusetts.

26. L. Mertz, Infrared Physics, 7, 17 (1967).

27. J. W. Cooley and J. W. Tukey, Mathematics of Computation, 19, 296 (1965).

28. J. B. Adams, Science 159, 1453 (1968).

29. J. B. Adams and T. B. McCord, J. Geophys. Res. 74, 4851 (1969).

30. "Micro Abrasives for Industry," Microabrasives Corporation, Westfield, Massachusetts, August 1, 1967.

31. NBS Test No. 212.14 - 11/67, April 11, 1967.

32. NBS Test No. 212.14 - 56/67, December 27, 1967.

33. M. J. D. Low and I. Coleman, Appl. Opt. 5, 1474 (1966).

34. H. W. Verleur, J. Opt. Soc. Am. 58, 1356 (1968).

35. J. C. Maxwell, A Treatise on Electricity and Magnetism, (Dover Publications, Inc. 1954) Vol. 1.